12-2004

Ab INITIO CALCULATION OF ELECTRONIC AND OPTICAL PROPERTIES OF BERYLLIUM CHALCOGENIDES (BeS, BeSe, AND BeTe) UNDER THE EFFECT OF PRESSURE

Aisha Ali Saif Bannan Al-Kaabi

Ab INITIO CALCULATION OF ELECTRONIC AND OPTICAL PROPERTIES OF BERYLLIUM CHALCOGENIDES (BeS, BeSe, AND BeTe) UNDER THE EFFECT OF PRESSURE

A Thesis Submitted to
The Dean of Graduate Studies of
The United Arab Emirates University

BY

Aisha Ali Saif Bannan Al-Kaabi

In Partial Fulfillment of The Degree of M.Sc in
Materials Science and Engineering

December 2004

Thesis Supervisor

Dr. Noureddine Amrane

Associate Professor of Materials Science
Physics
Department of Physics
Faculty of Science, UAEU-UAE

Examination Committee Members

Prof. J. Woods Halley
Professor of Materials Science
Department of Physics
Faculty of Science, Minnesota University-USA

Prof. Nacir Tit
Professor of Computational Physics
Department of Physics
Faculty of Science, UAEU-UAE

Table of Content

Acknowledgment

I am deeply indebted to Allah, for every thing, and for helping me in completing this work. Without his help this work would not be possible. Great thanks go to our father his highness Sheikh Zayed Bin Sultan Al Nahyan, the President of the United Arab Emirates who gave us the opportunity to study in the United Arab Emirates University to reach this level of education. I would like also to thank my supervisor Dr. Noureddine Amrane, not only for his guidance in writing this thesis, but also for his advice, concern, and encouragement during my study and research at the United Arab Emirates University. I would like to extend my appreciation to the members of my examination committee Pr. J. Woods Halley and Pr. Nacir Tit for their meticulous review and comments on my final draft. My heartfelt thanks go to my family for their relentless support in my academic study, especially my mother and my old sister for encouraging me all the time. My greatest debt is to my husband who gave me a huge support in this field.

I dedicate this thesis to my country and to all members of my family.

List of Figures

List of Tables

Abstract

There are several methods for materials simulation. Ab initio or first principles methods are used to solve the quantum mechanical equation which govern the behavior of a system. Ab inito calculation of the optical and electronic properties of solids is fundamental in solid state physics. APW+lo is used to examine different properties of BeS, BeSe, and BeTe. Beryllium compounds show different features in structure under different pressures, and they also show a phase transition from Zinc blende to Hexagonal NiAs. There is presently a great interest in the study of pressure induced phase transitions in II-VI semiconductors. Little is known about the ground state properties of Beryllium chalcogenides. The aim of this work is to examine the electronic and optical properties of these materials, with the emphasis on their dependence on hydrostatic pressure. First, we calculated the electronic properties such as band structure, charge density, density of state, and the contours of these materials, second we examined there optical properties such as refractive index, the dielectric function (both real and imaginary), and the coefficient of absorption under normal and transient pressure. Two packages -the Wien97 and the Wien2k- are used in our simulation.

CHAPTER I

Introduction

There are several methods for simulation of the material properties. All of these methods can be grouped into two categories, classical and quantum mechanical simulations. Each has its advantages and disadvantages. Classical simulations can handle a large number of atoms but have trouble dealing with the electrons, particularly defects such as an F-center which is the substitution of a negatively charged ion with an electron. They also require a lot of experimental data to fit the required empirical interatomic potentials. On the other hand, quantum mechanical calculations require very little experimental data but can only handle a small number of atoms, typically only a few tens of atoms. Molecular Dynamics simulations these days often use first principles calculations to fit force fields.

Ab initio or first principles methods, are used to solve the quantum mechanical Schrödinger equation which governs the behavior of a system. The only information which must be provided is the atomic numbers and positions of the atoms within the system. In contrast, empirical or semi-empirical approaches require a model of the interactions between the atoms to be supplied. The parameters of these models are usually derived by fitting the outcome of simulations to experimental data. Ab initio calculation of the optical and electronic properties of solids are reliable in solid state physics. These calculations provide a testing ground for well-developed theories such as the local density functional formalism [1].

Recent implementations of electronic structure methodologies can be divide into two groups. On one side, there are all-electron (AE) approaches which consider both core and valence electrons explicitly in the calculation. Since core electrons are strongly localized and the valence electrons are delocalized; these methods need suitable techniques such as augmented plane waves (APW) [2], linearized muffin tin orbitals (LMTO) [3], Slater type orbitals (STOs) [4], or Gaussian orbitals [5]. Alternatively, one can employ pseudo-potentials (PSPs) which effectively project out the core states from the problem while retaining the physical properties of the valence region. Many pseudo-potential applications use a plane-wave basis set but a variety of local orbital based implementations exist. The size of the basis set needed for a calculation of this type depends strongly on the shape of the atomic pseudo-potentials. Several approaches have

been proposed to construct soft pseudo-potentials which minimize the numerical cost of the computation.

Although the pseudo-potential method is extremely useful, there are reasons why alternatives could be attractive. Is the introduction of the pseudo-potential completely innocent? What do you do if you are interested in information that is inherently contained in the region near the nucleus (hyperfine fields for instance, or core level excitations)? Can the basis set be made more efficient? Therefore, we will search for a basis set that uses other functions than plane waves, and that does not require the introduction of a pseudo-potential. Such a basis set will have to be more efficient, but of course we do not want it to be biased. The successor will be the Augmented Plane Wave (APW) basis set.

In this work we use the Augmented Plane Wave combined with the local orbital (APW+lo). The ideas that lead to the APW basis set are very similar to what made us introduce the pseudopotential. In the region far away from the nuclei, the electrons are more or less `freely' (delocalized). Free electrons are described by plane waves. Close to the nuclei, the electrons behave quite as they did in a free atom, and they can be described more efficiently by atomic like functions. We concentrate our efforts in the theoretical study of optical and electronic properties of beryllium chalcogenides BeS, BeSe, and BeTe at normal pressure and under the effect of a hydrostatic pressure. The calculations are performed within the framework of density functional theory.

The Be compounds show features in structure and bonding very similar to the III-V semiconductor compounds. Each of these compounds crystallize at zero pressure in the zinc-blende (ZB) structure. Recent experiments and theoretical studies [6] reported the existence of a pressure induced structural phase transition of these compounds from the ZB to the hcp structure [7,8]. There is presently a great interest in the study of pressure induced phase transitions in II-VI compounds, among which the beryllium compounds stand. However, little is known about the ground state properties of the beryllium chalcogenides. These materials are potentially good for technological applications, mainly for blue-green laser diodes and laser-emitting diodes.

The purpose of our study is to analyze the optical and electronic properties of these elements at equilibrium and transition pressure.

The thesis is organized as follows: in the next chapter, a brief review of the many body problem and the density functional theory is presented. In chapter 3, the Ab initio pseudo-potential theory is extensively discussed. Chapter 4 deals with the different types of algorithms presented for minimizing total energy of Kohn-sham system. In chapter 5, we introduce the APW+lo method and we demonstrate the usefulness as well as the power of this method, and finally in chapter 6, we discuss our results and give our conclusion.

CHAPTER II

Density Functional Theory as a way to solve the quantum many body problem

II.1 The Many-body Problem

The macroscopic properties of all forms of matter are determined by quantum mechanical solutions of a many body Schrödinger equation governing the motion of the electrons and the nuclei [9].

The Schrödinger equation is the main equation given by:

$$H\psi = i\hbar\frac{\partial\psi}{\partial t} \qquad \text{(II.1)}$$

where H is the exact many-body Hamiltonian, and the wavefunction ψ is the function of the all electronic and nuclear coordinates.

Solving the Schrödinger equation is only part of the many–particle problem. As a matter of fact the aim here is not to get the eigenvalues and the eigenfunctions but rather use these latter to calculate some properties like the bonding energy, polarizability, conductivity, etc.., rather than the wavefunction itself [10].

A solid is a collection of heavy, positively charged particles (nuclei), and lighter, negatively charge particles (electrons). For a system containing N nuclei, there are N+ZN electromagnetically interacting particles. In this situation we are dealing with a problem called a many-body problem. The exact many-particle Hamiltonian for this system is:

$$\hat{H} = -\frac{\hbar^2}{2}\sum_i\frac{\nabla^2}{M_i} - \frac{\hbar^2}{2}\sum\frac{\nabla^2}{m_e} - \frac{1}{4\pi\varepsilon_o}\sum_{i,j}\frac{e^2 Z_i}{\left|\vec{R}_i - \vec{r}_j\right|} + \frac{1}{8\pi\varepsilon_o}\sum_{i\neq j}\frac{e^2}{\left|\vec{r}_i - \vec{r}_j\right|} + \frac{1}{8\pi\varepsilon_o}\sum_{i\neq j}\frac{e^2 Z_i Z_j}{\left|\vec{R}_i - R_j\right|} \qquad \text{(II.2)}$$

m_e and M_i is the mass of electrons and nuclei respectively. The first term is the kinetic energy operator for the nuclei, the second is for the electrons. The last three terms are the coulomb interaction between electrons and nuclei, between the electrons and other electrons, and between nuclei and other nuclei [11].

II.2 Level 1: The Born-Oppenheimer approximation

The Born Oppenheimer approximation [11,12] is the basis for the most of our thinking about shape and nuclear motion in polyatomic molecules. This approximation assumes that the nuclei in molecules are virtually standing still relative to the electrons. This is based on the small electronic-nuclear mass ratio, which is $\approx \frac{1}{1800}$ even for the closest case of atomic hydrogen

The nuclei are much heavier and therefore much slower than the electrons. Hence, the nuclei can be frozen at fixed positions, and we can assume them to be in instantaneous equilibrium with each other. The nuclei are reduced to a given source of positive charge, and become external to the electron cloud. Due to this approximation, a collection of NZ interacting negative particles moving in the potential of the nuclei is left.

The Born-Oppenheimer approximation states that, the nuclei do not move any more, hence, their kinetic energy is zero and the first term in the many-particle hamiltonian disappears. The last term reduced to a constant, the kinetic energy of the electron cloud is left [11].

The Hamiltonian can be written more compactly as

$$\hat{H} = \hat{T}_N(R) + \hat{T}_e(r) + \hat{V}_{eN}(r,R) + \hat{V}_{NN}(R) + \hat{V}_{ee}(r) \qquad \text{(II.3)}$$

where R is the set of nuclear coordinates and r is the set of electronic coordinates. If spin-orbit effects are important, they can be added through a spin-orbit operator $\hat{H}_{SO}$ [13].

Unfortunately, the $\hat{V}_{eN}(r,R)$ term prevents us from expressing $\hat{H}$ into nuclear and electronic parts, which would allow us to write the sample wavefunctions as a product of nuclear and electronic terms, $\psi(r,R) = \psi(r)\chi(R)$. The term $\hat{V}_{eN}(r,R)$ is large and can not be neglected; however, we can make the R dependence parametric, so that the total wavefunction is given as $\psi(r;R)\chi(R)$, we can fix R, the nuclear configuration, at some value R_a, and solve for the electronic wavefunction $\psi(r;Ra)$,

which depends only on R. We now show the mathematical details. First, $\hat{T}_N(R)$ can be neglected, and from the electrons point of view, the full Hamiltonian reduces to

$$\hat{H}_{el} = T_e(r) + \hat{V}_{eN}(r,R) + \hat{V}_{NN}(R) + \hat{V}_{ee}(r) \qquad \text{(II.4)}$$

$$\hat{H}_{el}\psi(r,R) = E_{el}\psi(r,R) \qquad \text{(II.5)}$$

this is called the "clamped-nuclei" Schrödinger equation. $\hat{V}_{NN}(R)$ is neglected in the above equation, which is justified to be just a constant which shifts the eigenvalues only by a constant amount. If we leave $V_{NN}(R)$ out of the electronic, Schrödinger equation leads to a similar equation

$$\hat{H}_e = \hat{T}_e(r) + \hat{V}_{eN}(r,R) + \hat{V}_{ee}(r) \qquad \text{(II.6)}$$

$$\hat{H}\psi(r,R) = E_e\psi_e(r,R) \qquad \text{(II.7)}$$

We will assume that $\hat{V}_{NN}(R)$ is included in the electronic Hamiltonian. Additionally, if spin-orbit effects are important, then they can be included at each nuclear configuration according to

$$\hat{H}_0 = \hat{H}_{el} + \hat{H}_{So} \qquad \text{(II.8)}$$

$$\hat{H}_0\psi(r,R) = E_0\psi(r,R) \qquad \text{(II.9)}$$

Consider the original Hamiltonian in (II.2). An exact solution can be obtained by using an expansion of the form

$$\psi = (r,R) = \sum_k \psi(r,R)\chi_k R \qquad \text{(II.10)}$$

although, to the extent that the Born-Oppenheimer approximation is valid, very accurate solutions can be obtained only for one or a few terms [14].

II.3 Level 2: Density Functional Theory

It is known that electrons in metals behave as more or less free objects [10,15]. In a classical liquid, the description is not in terms of individual particles positions and

momenta, but in terms of densities and velocity fields. A similar approach can actually be taken for electrons, which is called Density Functional Theory (DFT) [15-19]. DFT methods are currently implemented in most of commercial ab initio program packages [20].

II.3.1 Limitations

Despite the remarkable success of the LDA [20,21], its limitations impose that caution must be used in its application. For systems where the density varies slowly, the LDA tends to perform well, and chemical trends are well reproduced. In strongly correlated systems, an independent particle picture breaks down, the LDA is very inaccurate. For example, the transition metal oxides XO (X =Fe, Mn, Ni) are almost all insulators, but the LDA predicts that they are either semiconductors or metals. More over, the LDA has been applied to high T_c superconductors, but finds several to be metallic, when in reality they are insulating at 0 Kelvin.

It is a well-known trend that the LDA underestimates the bandgaps. This does not affect its success and reliability for the ground state properties. Among other LDA limitations we mention the following: the LDA finds the wrong ground state for many simpler cases. For example, the LDA finds the wrong ground state for the titanium atom. The LDA does not account for van der Waals bonding, and gives a very poor description of hydrogen bonding. These phenomena are essential for most of biochemistry compounds: the structure of DNA depends critically on hydrogen bonding, as do the changes in the structure of most molecules on salvation.

An obvious approach to improving the LDA is to include gradient corrections by making the energy functional a functional of the energy and its gradient:

$$E_{XC}^{GGA}[\rho(\vec{r})] = \int \varepsilon_{XC}(\rho(\vec{r}))\rho(\vec{r})dr + \int F_{XC}[\rho(\vec{r}), |\nabla\rho(\vec{r})|]dr \quad \text{(II.11)}$$

where F_{XC} is a correction chosen to satisfy one or several known limits for E_{XC}.

We emphasize that there is no unique recipe for F_{XC}, and several dozen functionals have been proposed in the literature. They do not always represent a systematic improvement over the LDA and results must be carefully inspected.

II.3.2 The Choice of a Basis Set Plane Waves

The Kohn-Sham orbitals, ψ_i, may be represented in terms of any complete basis set. For this task, many choices are possible i.e. atomic orbitals, Gaussians, LAPW and plane waves. This latter is the basis set we use in practice. The use of a plane wave (PW) basis set offers a number of advantages, including the simplicity of the basis functions, which make no preconceptions regarding the form of the solution. It also yields the ability to efficiently calculate the forces on atoms.

In general, the representation of an arbitrary orbital in terms of a PW basis set would require a continuous, and hence infinite, basis set. However, the implementation of periodic boundary conditions allows the use of Bloch's Theorem whereby the ψ_i may be written

$$\psi_{i,k}(r) = \sum_G C_{i,k}(G) e^{i(K+G)r} \qquad \text{(II.12)}$$

where the sum is over reciprocal lattice vectors G and K is a wave vector which lies within the first Brillouin zone. Thus, the basis set for a given K will be discrete, although in principle it will still be infinite. In practice, the set of plane waves is restricted to a sphere in reciprocal space most conveniently represented in terms of a cut-off energy, E_{cut}, such that for all values of G used in the expansion

$$\frac{\hbar^2 |K+G|^2}{2m_e} \leq E_{cut} \qquad \text{(II.13)}$$

Thus, the convergence of the calculation with respect to basis set may be ensured by variation of a single parameter, E_{cut}. This is a significant advantage over many other basis set choices, with which the calculated properties often show extreme sensitivity to small changes in basis set and no systematic scheme for convergence would be available.

The choice of periodic boundary conditions is natural in the case of bulk solids which exhibit perfect translational symmetry.

The electron density $\rho(\vec{r})$ and energy are given by averaging the results for all values of K in the first Brillouin zone.

$$\rho(\vec{r}) = \frac{1}{V} \int \rho(k) d^3K \qquad \text{(II.14)}$$

where

$$\rho_K(\vec{r}) = \sum_{i=1}^{N} \left|\psi_{i,k}(\vec{r})\right|^2 \qquad \text{(II.15)}$$

and

$$E = \frac{1}{V}\int E(K)d^3K \qquad \text{(II.16)}$$

Where E is the energy of the electron

In an extended system, these integrals are replaced by weighted sums over a discrete set of K-points which must be carefully selected to ensure convergence of the results. An isolated molecule will exhibit no dispersion, i.e.. there will be no variation of E and $\rho(\vec{r})$ with K. Therefore, these properties need only be calculated at a single K-point. There has been significant discussion regarding the optimal choice of K-point for performing calculations on isolated systems.

The principle disadvantage of the use of a PW basis set is the number of basis functions required to accurately represent the Kohn-Sham orbitals. This problem may be reduced by the use of pseudopotentioals as described in the next chapter, but several hundred basis functions per atom must still be used, compared with a few tens of basis function with the use of some atom-centered basis sets

II.3.3 The theorems of Hohenberg and Kohn

In the year 1964 Hohenberg and Kohn published in physical Review two fundamental theorems which gave birth to the modern density functional theory, an alternative approach to deal with the many body problem in electronic structure theory [22].

Since the formulation of quantum mechanics in the 1920s, two major approaches have emerged for the computation of the properties of atoms, molecules and solids: Hartree-Fock theory [12,22,23] and density functional theory. The Hartree-Fock and related methods have been most popular in the quantum chemistry community, while density functional theory has been the main method used for calculations of solids [9].

Density functional theory is an extremely successful approach for the description of ground state properties of metals, semiconductors, and insulators. The success of density functional theory not only encompasses standard bulk material but also complex

materials. Density functional theory DFT is based on the notion of the single particle electron density as a fundamental variable. This is a consequence of the Hohenberg-Kohn theorem [21,22] which states that the ground state electron energy may be found by minimizing the expectation value of the total energy regarded as a functional of the electron density $\rho(\vec{r})$.

The traditional formulation of the two theorems of Hohenberg and Kohn [18] is as follows: The first Hohenberg-Kohn theorem, as published in 1964, states that there is a one-to-one correspondence between the ground state density $\rho(\vec{r})$ of a many-electron system and the external potential V_{ext}. In other words, the external potential $V_{ext}(\vec{r})$ is a unique functional of the density $\rho(\vec{r})$; since, in turn $V_{ext}(\vec{r})$ fixes $\hat{H}$ and we see that the full many particle ground state is a unique functional of $\rho(\vec{r})$.

$$V_{ext}(\vec{r}) => \rho(\vec{r}) \qquad \text{(II.17)}$$

and the inverse mapping exists

$$\rho(\vec{r}) => V_{ext}(\vec{r}) \qquad \text{(II.18)}$$

Every property could be calculated with the help of $\rho(\vec{r})$, since the density $\rho(\vec{r})$ contains all the information of the system [22].

The proof of the Hohenberg-Kohn HK1 is based on reduction and runs as follows: Suppose that we have two different external potentials $V_{ext}(\vec{r})$ and $V_{ext}(\vec{r})'$ with the same ground state density $\rho(\vec{r})$

$$V_{ext}(\vec{r}) \neq V_{ext}(\vec{r})' \qquad \text{(II.19)}$$

The two external potentials lead to two different Hamiltonians with two different ground state wavefunctions ψ

$$H = H_0 + V_{ext} \qquad H\psi = E\psi \qquad \text{(II.20)}$$

$$H' = H_0 + V'_{ext} \qquad H'\psi' = E'\psi' \qquad \text{(II.21)}$$

Therefore ψ and ψ' are different N particle wavefunctions. Using the variational principle we can write

$$E = \langle \psi | \hat{H} | \psi \rangle < \langle \psi' | \hat{H} | \psi' \rangle = \langle \psi' | H' | \psi' \rangle + \langle \psi' | \hat{H} - \hat{H}' | \psi' \rangle \qquad \text{(II.22)}$$

Since, the two Hamiltonians differ only by the external potential we can write

$$E < E' + \langle \psi' | V_{ext} - V_{ext}' | \psi \rangle \qquad \text{(II.23)}$$

which yields

$$E < E' + \int \rho(\vec{r}) \{ V_{ext} - V_{ext}' \} d\vec{r} \qquad \text{(II.24)}$$

The external field interacts only via a classical electrostatic interaction between the electrons and the nuclei.

We interchange the primed and the unprimed quantities and we will repeat the same steps above which leads to

$$E' < E + \int \rho(\vec{r}) \{ V'_{ext} - V_{ext} \} d\vec{r} \qquad \text{(II.25)}$$

Then

$$E' + E < E + E' \qquad \text{(II.26)}$$

which means that, there cannot be two different external potentials V_{ext} and V_{ext}' that yield the same density $\rho(\vec{r})$.

Since the complete ground state energy E_0 is a unique functional of the density ρ, we can write

$$E_0(\rho) = T(\rho) + V_{\text{int}}(\rho) + V_{ext}(\rho) \qquad \text{(II.27)}$$

The previous expression can be divided into two parts, system dependent $V_{ext}(\rho)$, and system independent $T(\rho) + V_{\text{int}}(\rho)$. The system dependent part, depends on the actual system determined by the external potential, and the system independent part defines the Hohenberg-Kohn functional

$$F_{HK}(\rho) = T(\rho) + V_{\text{int}}(\rho) \qquad \text{(II.28)}$$

The second Hohenberg-Kohn theorem states that:

$$E_g \leq E(\tilde{\rho}) = T(\tilde{\rho}) + V_{\text{int}}(\tilde{\rho}) + V_{ext}(\tilde{\rho}) \qquad \text{(II.29)}$$

where $\tilde{\rho}$ is the density associated to a N electron system with external potential V_{ext}, valid only if $\tilde{\rho} = \rho$ [22].

II.3.4 The Kohn-Sham equations

While the Hohenberg-Kohn theorem shows that it is possible to use the ground state density to calculate properties of the system, it does not provide a way of finding the ground state density. This is provided by the Kohn-Sham equations [24].

The Kohn-Sham theory is considered as the most practical method for calculating the electronic structure of materials [7].

The main advantage of the Kohn-Sham method is that it allows a straightforward determination of a large part of the kinetic energy in a simple way. Another advantage, it provides a self-consistent one particle picture including correlations of interacting electronic systems, which provides a basis for the one-particle arguments used in solid state physics and chemistry to explain and predict certain properties of chemical bonding [10].

If we return back to Hohenberg-Kohn functional, both known and unknown parts can be identified

$$F_{HK}T + V_{ee} \tag{II.30}$$

with potential energy term

$$V_{ee}\frac{1}{2}\iint\frac{\rho(\vec{r}_1)\rho(\vec{r}_2)}{r_{12}}d\vec{r}_1 d\vec{r}_2 + E_{NCL}(\rho) = J(\rho) + E_{NCL}(\rho) \tag{II.31}$$

where $J(\rho)$ is classical interaction of two charge densities and $E_{NCL}(\rho)$ contains all non classical parts. Thus the complete energy functional is given by:

$$E[\rho] = T[\rho] + J[\rho] + E_{NCL}[\rho] + \int V_{ext}\rho(\vec{r})d\vec{r} \tag{II.32}$$

The basic problem is the unknown functional for the kinetic energy. Kohn and Sham published a paper in 1953 to solve this problem, where they suggested to split this functional into two parts.

$$T[\rho] = T_S[\rho] + T_C[\rho] \tag{II.33}$$

where $T_S[\rho]$ will be the expressed in a one particle approach similar to Hartree-Fock, and the second part, which is the unknown part contains the difference between the real

functional $T[\rho]$ and the one particle term $T_S[\rho]$, which will be treated as well as the other. The remaining parts of the total energy functional are also unknown. We can write

$$E[\rho] = T_S[\rho] + J[\rho] + V_{ext}[\rho] + E_{NCL}[\rho] + T_C[\rho] \qquad \text{(II.34)}$$

$$= T_S[\rho] + J[\rho] + V_{ext}[\rho] + E_{XC}[\rho]$$

$E_{XC}[\rho]$ called the exchange-correlation functional, which remains unknown. $T_S[\rho]$ is defined as

$$T_S[\rho] = -\frac{1}{2}\sum_i \langle\ \theta_i | \nabla^2 | \theta_i\ \rangle \qquad \text{(II.35)}$$

where θ_i are one particle wavefunctions, which are determined by applying the variation principle, which leads finally to the Kohn-Sham equations

$$\hat{f}^{KS}\theta_i = e_i\theta_i \qquad \text{(II.36)}$$

with the Kohn-Sham operator

$$\hat{f}^{KS} = -\frac{1}{2}\nabla^2 + \int\frac{\rho(\vec{r}_2)}{r_{12}}d\vec{r}_1 + V_{XC}(\vec{r}_1) + \sum_A \frac{Z_A}{r_{1A}} \qquad \text{(II.37)}$$

$$= -\frac{1}{2}\nabla^2 + V_S(\vec{r}_1)$$

This shows that the Kohn-Sham equations provide a method of obtaining the kinetic energy functional and also minimizes the energy functional. In general, the method only provides the total energy as well as the ground state electron density [25].

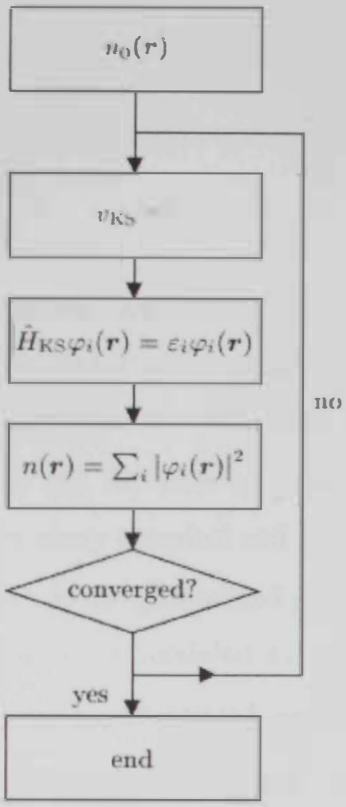

Figure 2.1: Flow chart for computing the wavefunctions

II.3.5 The exchange-correlation functional

The Local Density Approximation (LDA) introduces the form of the exchange correlation functional [12,26] as

$$E_{XC}^{LDA} = \int \rho(\vec{r})\varepsilon_{XC}(\rho(\vec{r}))d\vec{r} \qquad (II.38)$$

The previous form means that the exchange-correlation energy due to a particular density $\rho(\vec{r})$ could be found by dividing the material in infinitesimally small volumes with a constant density. Each such volume participates in the total exchange correlation energy by an amount equal to the exchange correlation energy of an identical volume filled with a homogeneous electron gas that has the same overall density as the original material has in this volume [11].

The ε_{XC} is the exchange correlation energy per particle of a uniform electron gas. This quantity can be further split into two parts:

$$\varepsilon_{XC}(\rho(\vec{r})) = \varepsilon_X(\rho(\vec{r})) + \varepsilon_C(\rho(\vec{r})) \qquad \text{(II.39)}$$

For example, the exchange part $\varepsilon_X(\rho(\vec{r}))$ can be derived analytically and reads as

$$\varepsilon_X(\rho(\vec{r})) = -\frac{3}{4}\sqrt[3]{\frac{3\rho(\vec{r})}{\pi}} \qquad \text{(II.40)}$$

The correlation part cannot be derived analytically, but can be calculated numerically with high accuracy by means of Monte Carlo simulations [10].

In the Local Density Approximation LDA, the XC hole $\rho_{XC}(r,r')$ about an electron at r is approximated by the XC hole of a uniform electron gas of density $\rho = \rho(\vec{r})$. This is not enough for many chemical and biological applications. The most widely used correction to the LDA is the generalized gradient approximation GGA [27] in which the effects of homogeneity are modeled using the semi local approximation $E_{XC} = \int drf(\rho, |\nabla\rho|)$ where f is some parameterized nonlinear function of ρ and $\nabla\rho$.

A common feature of all current GGA is that their construction is guided by limiting behaviors and sum rules, they are designed to fit various integrated quantities such as total exchange energies of atoms or ionization energies of molecules, but incorporate little or no information about the behavior of local quantities such as $\rho_{XC}(r,r')$ and the exchange correlation energy density $e_{XC}(r)$ in strongly inhomogeneous systems [28].

CHAPTER III

The Pseudopotential Method

III.1 Introduction

Nowadays, the pseudopotential method [29] of a solid is implemented using modern computers. It paved the way in providing workable models and simulations. It is now possible to predict accurately the properties of complex systems such as semiconductors, liquids with hundreds, if not thousands of atoms. The pseudopotential model treats this matter as a sea of valence electrons moving in a background of ion cores. The cores are composed of nuclei and inner-core electrons. This model avoids many complexities that could be encountered in the electron model. For example, a group IV solid, such as C (with 6 electrons) is treated in similar way as Pb (with 82 electrons) since both have 4 valence electrons [30]. Pseudopotential calculations focuses on the accuracy of the valence electron wavefunction in the special region away from the core. The smoothly varying pseudo wavefuction is taken to be identical to the appropriate all-electron wavefunction in the chemically active bonding region.

Pseudopotentials are very important components of first principles calculations as they remove the need to consider core electrons, but rather take into account only the valence electrons. The pseudo-wavefunction is a much simpler and smoother function to approximate than all-electron wavefunction. The justification for the use of a pseudopotential lies in the fact that the highly localized core wavefunction cannot take part in the bonding of atoms. Nevertheless, the valence electrons undergo exchange interactions with core ones and this makes the problem of constructing pseudopotentials non trivial [11].

III.2 Construction of the Pseudopotential

A number of schemes have been developed to construct pseudopotentials that yield wavefunctions. As previously mentioned, most modern pseudopotentials are based on the same idea, but are not fit to experimental data. Rather, they are based on density functional theory. Within this framework, it is easy to apply the pseudopotental approach to a wide variety of problems [11].

III.3 Empirical schemes

We have focused our effort in this work on the ab-initio method, and their outstanding predictive power. Nevertheless, computing cost are the main handicaps and in this matter, methods such as the empirical pseudopotental, tight binding, classical molecular dynamics, etc... have been giving results that are correct with less computing time and system constraints. The empirical pseudopotentail method has revealed so far quite satisfactory results for the semiconductor materials. In these perspectives, it also has a predictive power, even though it relies on experimental results as input such as (energy gaps) in its reliability.

III.3.1 Empirical Pseudoptential method

The empirical pseudopotential method (EPM) [31,32] has been extensively applied to the diamond and zinc-blende semiconductors. Studies on these latter materials have been based on local approximations. In this approach, reflectivity experiments have played a prominent role in determining the theoretical parameters needed in the EPM calculations. The local approximation has been proven to be efficient to explain most of the optical data available for semiconductor compounds. However, if we extend the early calculations, which have invoked the local pseudopotential approximation to the valence bands, and compare the results to experiment some discrepancies arise. Specifically, high resolution photoemission results (XPS) and ultraviolet photoemission spectroscopy (UPS) have demonstrated that local EPM calculations obtain incorrect valence bandwidths, in the majority of cases, as compared with experiment. Experimental advances using x-rays have permitted an assessment of the pseudopotential charge densities. While the experimental data for Si indicated that the local pseudopotential yielded a correct bonding-charge, the bond shape was incorrect. Also X-ray data on InSb indicated the local pseudopotential approach overestimates the ionicity of the crystal, i.e., it yields a greater charge transfer from In to Sb than indicated by the experiment.

Owing to the nature of these discrepancies, it was speculated that a purely local pseudopotential technique could not yield satisfactory results, and nonlocal pseudopotential should be considered. This evidence for this reasoning was reinforced particularly by the valence band width discrepancy, because other one-electron

approaches (which corresponded to energy dependent non local pseudopotential) tended to yield more accurate valence bands than the local EPM approach.

III.3.2 Non local Pseudopotentials

The fundamental concept invoked in a pseudopotential calculation is that the ion core can be omitted. Computationally this is crucial as the deep core potential has been removed and a simple plane wave basis set would yield rapid convergence. Simply stated, we rewrite the one-electron Hamiltonian as

$$H = \frac{P^2}{2m} + V_p(\vec{r}) \qquad \text{(III.1)}$$

If many atomic species are present, let R_j^{α} is the position of the jth atom of the αth species. These equations may be specified, for instance, in the case of the diamond or zinc-blende compounds, ($A^N B^{8-N}$) to

$$V(\vec{G}) = V^S(\vec{G})\cos(\vec{G}.\vec{\tau}) + iV^A(\vec{G})\sin(\vec{G}.\vec{\tau}) \qquad \text{(III.2)}$$

where

$$V_s(\vec{G}) = \frac{1}{2}\left[V_A(\vec{G}) + V_B(\vec{G})\right] \qquad \text{(III.3)}$$

$$V_a(\vec{G}) = \frac{1}{2}\left[V_A(\vec{G}) - V_B(\vec{G})\right]$$

τ=1/4a(1,1,1), where a is the lattice constant. V^S and V^A are the symmetric and antisymmetric form factors, respectively.

The local empirical pseudopotential method is based upon the above simplification. If we take the pseudopotentials to be spherical so that $V^{\alpha}{}_P(r) = \left|V^{\alpha}{}_P(r)\right|$, the form factors depend upon the magnitude of G, with a corresponding reduction in the number of form factors. These form factors are the empirically determined parameters fit to experimental data such as optical gaps.

We may write a non local (NL) correction term to the local atomic potential term of the form

$$V^{\alpha}{}_{NL}(\vec{r}, E) = \sum_{l=0}^{\infty} A_l(E) f_l(\vec{r}) P_l \qquad \text{(III.4)}$$

where $A_l(E)$ is an energy dependent depth, $f_l(\vec{r})$ is a function simulating the effect of core states with l-symmetry, and P_l is a projection operator for the *l-th* angular momentum component. Only l = 0, 1 are significant, so we may write (symbolically)

$$s + p + d \cong l \tag{III.5}$$

and need to consider, for example, s and d terms. Model potentials calculations indicate a weak energy dependence for the $A_l(E)$, where l = 1 or 2. To choose a form for $f_l(\vec{r})$ we employ a square well, a form which has the advantage of simplicity and wide applicability. Hence

$$f_l(r) = \begin{cases} 1, r & for < R_l \\ 0, r & for \geq R_l \end{cases} \tag{III.6}$$

with a plane wave basis set the required matrix elements are of the form

$$V_{NL}(\vec{K},\vec{K}') = \frac{4\pi}{\Omega_a}\sum_{l,i} A_l^i(E)(2l+1)P_l(\cos(\theta_{KK}'))\times S^i(\vec{K}-\vec{K}')F_l^i(\vec{K},\vec{K}') \tag{III.7}$$

where $\vec{K} = \vec{k} + \vec{G}, and\ \vec{K}' = \vec{k} + \vec{G}'$,

$$F_l(K,K') = \begin{cases} 1/2R^2\left\{[j_l(KR)]^2 - j_{l-1}(KR)j_{l+1}(KR)\right\}, & for\ K = K' \\ \left[R^2/(K^2-K'^2)\right]\left[Kj_{l+1}(KR)j_l(K'R) - K'j_{l+1}(K'R)j_l(KR)\right], & for\ K \neq K' \end{cases} \tag{III.8}$$

The $j_l(x)$ are the spherical Bessel functions, $P_l(x)$ are the Legendre polynomials and i is a sum over the atomic species present.

To simulate energy dependence for the s-states we make the approximation for the matrix elements between K and K' as follow:

$$A_0(E)\alpha_0 + \beta_0\left\{\left[E^0(K)E^0(K')\right]^{1/2} - E^0(K_F)\right\}, \tag{III.9}$$

where $E^0(K) = \hbar^2K^2/2m$. This approximation works quite well compared to more rigorous techniques. The parameters required by our potential were fixed by detailed comparisons with experimental reflectivity and photoemission data. Unfortunately, the

addition of a non-local correction term increases the number of parameters rather dramatically.

III.4 Band Structure

Once the potential is determined, it is a straightforward calculation to solve for the energy band spectrum. The eigenvalues and eigenvectors are found by solving the secular equation for the effective one electron Hamiltonian matrix

$$H_{\vec{K}\vec{K}'} = \frac{\hbar^2}{2m} K^2 \delta_{\vec{K}\vec{K}} + [V^S(|\vec{K}-\vec{K}'|) + V_{NL}^S(\vec{K},\vec{K}')]\cos[(\vec{K}-\vec{K}).\vec{\tau}]$$
$$+ i[V^A(|\vec{K}-\vec{K}'|) + V_{NL}^A(\vec{K},\vec{K}')]Sin[(\vec{K}-\vec{K}').\vec{\tau}'] \qquad \text{(III.10)}$$

The spin-orbit Hamiltonian matrix element contribution to the Hamiltonian is written as

$$H_{GG}^{SO}(k) = (K \times K').\sigma_{ss'} \left\{ -i\lambda^S \cos[(G-G').\tau] + \lambda^A \sin[(G-G').\tau] \right\}$$

where $K=k+G$ and $K'=k+G'$, $\sigma_{ss'}$ is the Pauli spin matrix, λ is a quantity which represents the strength of the spin interaction, similar to the pseudopotential form factor.
Where

$$\lambda^{SA} = (\lambda 1 + \lambda 2)/2 \qquad \text{(III.11)}$$

$$\lambda_1(K,K') = \mu B_{n1}(K) B_{n1}(K') \qquad \text{(III.12)}$$

$$\lambda_2(K,K') = \alpha\mu B_{n1}(K) B_{n2}(K') \qquad \text{(III.13)}$$

Atoms undergo small displacement u_{ia} from their equilibrium positions R_{ia}. Within this model we can compute both energy shifts caused by strains. It remains however that this model is certainly not exact. Nevertheless, to first order in the displacement u_{ia} it seems often to be an excellent approximation.

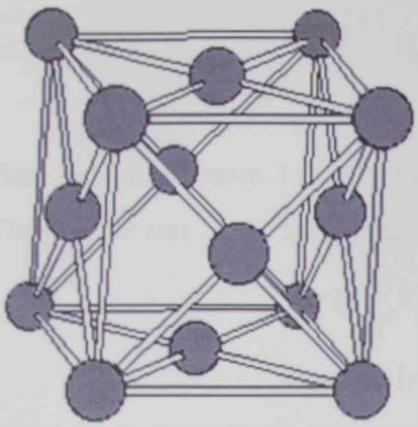

Figure 3.1.a: FCC Crystal Structure

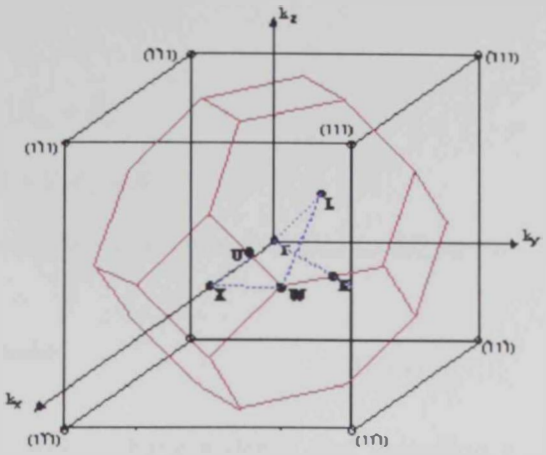

Figure 3.1.b: Brillouin zone of the FCC lattice

III.4.1 Static energy shift

The energy eigenvalues ε_{kn} of perfect and strained crystals are given by:

$$\det\left\{\left|(\vec{k}+\vec{G}_1)-\varepsilon_{\vec{k}n}\right|\delta(\bar{\bar{G}}_1,\bar{\bar{G}}_2)+V(\bar{\bar{G}}_1+\bar{\bar{G}}_2)\right\}=0,$$

$$\det\left\{\left|(\vec{k}'+\vec{G}'_1)-\varepsilon_{\vec{k}n}\right|\delta(\bar{\bar{G}}'_1,\bar{\bar{G}}'_2)+V(\bar{\bar{G}}'_1+\bar{\bar{G}}'_2)\right\}=0$$

The plane wave representation is used only for convenience. It is not assumed that there is a weak pseudopotential is necessarily viable for an actual calculation. Primes are used to denote quantities in the strained crystal. They are given for lattice vectors $\vec{R}_t$ and for reciprocal lattice vectors $\vec{G}_t$. The unit-cell volume is:

$$(\vec{R}_1\times\vec{R}_2).\vec{R}_3=\Omega_c\rightarrow\Omega'_c=(1+trS)\Omega_c$$

The potential of the unstrained crystal has a fourier transform given by

$$V(\vec{G})\equiv\frac{1}{\Omega}\int d\vec{r}e^{-i\vec{G}.\vec{r}}\sum_a V_a(\vec{r}-\vec{\tau})$$

$$=\sum_a V_a(\vec{G})e^{-i\vec{G}.\vec{\tau}a}$$

To work out the corresponding quantity for the strained crystal, we need an explicit formula for the location of the atoms:

$$R_{ia} \rightarrow R'_{ia} = (\underline{1} + \underline{S})\vec{R}_{ia} + \vec{\delta}_a$$

$$= \vec{R}'_i + (\underline{1} + \underline{S})\vec{\tau}_a + \vec{\delta}_a$$

Here δa is the "internal shift" of atom coordinates within a cell which is due to the strain. The Fourier transform for the strained crystal is:

$$V(\vec{G}') = (1 - tr\underline{S})\sum_a V_a[(1 - \underline{S})\vec{G}]e^{-i\vec{G}\cdot(\vec{\tau}a + \vec{\delta}a)} \qquad \text{(III.14)}$$

The empty core model is used to allow a well to have a depth and including a screening factor. The atomic pseudopotential is given in real space by

$$V_i(r) = \begin{cases} -A & r < R \\ -Z_i r^{-1} e^{-\alpha_j' r} & r > R \end{cases} \qquad \text{(III.15)}$$

where the factor $e^{-\alpha_j' r}$ represents screening of the potential due to other electrons. The Fourier transform of the pseudopotential is given by:

$$Vi(G) = -\frac{8\pi}{\Omega ij}\left[\frac{Z_i e^{-\alpha R_i}}{G2 + \alpha_i^2}\left(\cos GR_i + \frac{\alpha_i}{G}\sin GRi\right) + \frac{Ai}{G3}(\sin GR_i - GR_i \cos GR_i)\right] \qquad \text{(III.16)}$$

Where Ω_{ij} is the volume of the unit cell of the binary compounds formed by elements i and j. All quantities are given in atomic units. We obtain the symmetric and antisymmetric form factors of a binary system which contains eight parameters: A_i, Z_i, α_i, and R_i $(i=1, 2)$. We then perform the least squares fit the function simultaneously to the symmetric and antisymmetric form factors of the given binary crystal. The parameters are adjusted to get the best fit to these form factors.

CHAPTER IV

The Minimizations of the Kohn-Sham energy Functional

IV.1 Periodic systems

In contrast to the single-particle picture, previously discussed, one must overcome other difficulties such as the interaction between the electrons. The formidable task which remains task is the handling of a very large number (infinite) of non-interacting electrons moving in the static potential of a large number of the nuclei or ions. Two difficulties must be overcome: (i) the wave function must be calculated for each of the large number of electrons in the system, and (ii) each electronic wave function extends over the entire solid, and the basis set required to expand each wave function is infinite. Performing calculations on periodic systems and applying Bloch's theorem to the electronic wave function can surmount both problems.

IV.2 Bloch's theorem

Bloch's theorem [33] states that in a periodic solid each electronic wave function can be written as the product of a cell periodic part and a wave like part

$$\psi_i(\vec{r}) = \exp[ik.r] f_i(\vec{r}) \qquad \text{(IV.1)}$$

The cell periodic part of the wave function can be expanded using a basis set consisting of a discrete set of plane wave whose wave vectors are reciprocal lattice vectors of the crystal,

$$f_i(\vec{r}) = \sum_G c_{j,G} \exp[i\vec{G}.\vec{r}] \qquad \text{(IV.2)}$$

where the reciprocal lattice vectors G are defined by $Gl = 2\pi m$ for all l, where l is a lattice vector of the crystal and m is an integer. Therefore each electronic wave function can be written as a sum of plane waves,

$$\psi_i = \sum_G c_{j,k+G} \exp[i(\vec{k} + \vec{G}).\vec{r}] \qquad \text{(IV.3)}$$

IV.3 k-point sampling

Electronic states are allowed only at a set of k points determined by the boundary conditions that apply to the bulk solid. The density of allowed k points is proportional to the volume of the solid. The infinite number of electrons in the solid are accounted for by an infinite number of k points, and only a finite number of electronic states are

occupied at each k point. The Bloch theorem changes the problem and reduce it to calculating a finite number of electronic wave functions at an infinite number of k points. The occupied states at each k point contribute to the electronic potential in the bulk solid so that, in principle, an infinite number of calculations are needed to compute this potential.

However, the electronic wave functions at k points that are very close together will be almost identical. Hence it is possible to represent the electronic wave function over a region of k space by the wave functions at a single k points are required to calculate the electronic potential and hence determine the total energy of the solid.

Methods have been devised for obtaining very accurate approximations to the electronic potential and the contribution to the total energy from a filled electronic band, by calculating the electronic states at special sets of k points in the Brillouin zone [34-36] Using these methods one can obtain an accurate approximation for the electronic states using a very small number of k points.

The magnitude of the error in calculating the total energy can always be reduced by using a denser set of k-points; or selecting a suitable technique such as: Monkhorst-pack, or tetrahedron methods etc...

IV.4 Plane wave basis set

Bloch's theorem states that the electronic wave functions at each k point can be expanded in terms of a discrete plane wave basis set. In principle, an infinite plane wave basis set [37] is required to expand the electronic wave functions. However, the coefficients C_j for the plane waves with small kinetic energy $\hbar^2 / 2m|k+G|^2$ are typically more important than those with larger kinetic energy. Thus the plane wave basis set can be truncated to include only plane waves that have kinetic energies less than some particular cutoff energy. The truncation of the plane wave basis set at a finite energy cutoff will lead to an error in the computed total energy. However, it is possible to reduce the magnitude of the error by increasing the value of the cutoff energy. It is common practice to increase the cutoff energy until the calculated total energy has converged.

IV.5 Plane wave representation of Kohn-Sham equations

When plane waves are used as a basis set for the electronic wave functions, the Kohn-Sham equations assume a particularly simple form.

The integration over r gives:

$$\sum_{G'}\left[\frac{\hbar^2}{2m}|k+G|^2\,\delta_{GG'}+V_{ion}(G-G')+V_H(G-G')+V_{XC}(G-G')\right]c_{i,k+G'} = \varepsilon_i c_{i,k+G} \qquad \text{(IV.4)}$$

In this form, the kinetic energy is diagonal, and the various potentials are described in terms of their Fourier transforms.

IV.6 Direct Minimization of the Kohn-Sham energy Functional

For the calculation of the Kohn-Sham(KS) ground state, it is possible to discriminate between two methods. (i) Methods for determining the minimum of the KS total energy functional directly (called direct methods) and (ii) iterative methods for diagonalizing the KS Hamiltonian in conjunction with an iterative improvement (i.e., mixing) of the charge density or the potential (These methods are called self-consistent methods).

Both methods require no explicit storage of the Hamiltonian matrix and should therefore show similar efficiency. The direct methods (i) have been pioneered by Car and Parrinelo. They are based on the fact that the Kohn-Sham energy functional is minimal at the electronic ground state. Therefore, minimization with respect to the variational degrees of freedom leads to a convenient scheme for calculating the electronic ground state. The original scheme of Car and Parrinelo have been so far improved. Improvements might be obtained by introducing an improved preconditioning for the gradient or by replacing the second order CP equations by first order steepest descent equations. We are using the self consistent method for finding the KS ground state.

In this respect conjugate gradient(CG) schemes are very promising. Within these schemes the KS functional is minimized along a given search direction exactly, and in successive steps the new search direction is conjugated to previous search directions.

In this section the methods that allow direct minimization of the Kohn-Sham energy functional in a tractable and efficient manner are described. There are an infinite number

of Kohn-Sham Hamiltonians, each of which has a different set of eigenstates. One of these sets of eigenstates the set generated by the Kohn-Sham Hamiltonian, minimizes the Kohn-Sham energy functional. This is useful when we calculate the relaxation of the atomic position which we did not do in this work.

IV.7 The Hellmann-Feynman theorem

The force on ion I, f_I, is minus the derivative of the total energy of the system with respect to the position of this respective ion

$$f_I = -\frac{dE}{dR_I} \tag{IV.5}$$

As the ion moves from one position to another, the wave function must change to the self-consistent Kohn-Sham eigenstated corresponding to the new position of the ion if the value of the Kohn-Sham energy functional is to remain physically meaningful. The changes in the electronic wave functions contribute to the force on the ion, as clearly can be seen by expanding the total derivative:

$$f_I = -\frac{\delta E}{\delta R_I} - \sum_i \frac{\delta E}{\delta \psi_i}\frac{\delta \psi_i}{dR_I} - \sum_i \frac{\delta E}{\delta \psi_i^*}\frac{\delta \psi_i^*}{\delta R_I} \tag{IV.6}$$

It can be seen that the force is only the partial derivative of the Kohn-Sham energy functional with respect to the position of the ion. In the Lagrange equations of motion for the ion, the force on the ion is not a physical force. It is an effective force that the ion would experience from a particular electronic configuration. However, it is easy to show that when each electronic wave function is an eigenstate of the Hamiltonian the final two terms sum to zero. Since $\frac{\delta E}{\delta \psi_i^*}$ is just $H\psi_i$, these two can be written

$$\sum_i \left\langle \frac{\delta \psi_i}{\delta R_I} \middle| H\psi \right\rangle + \sum_i \left\langle H\psi_i \middle| \frac{\delta \psi_i}{\delta R_i} \right\rangle \tag{IV.7}$$

However, if each ψ_i is an eigenstate of the Hamiltonian,

$$H\psi_i = \lambda_i \psi_i,$$

then

$$\sum_i \left\langle \frac{\delta\psi_i}{\delta R_I} \middle| H\psi_i \right\rangle + \sum_i \left\langle H\psi_i \middle| \frac{\delta\psi_i}{\delta R_I} \right\rangle = \sum_i \lambda \frac{\delta}{\delta R_I} < \psi_i | \psi_i >= 0 \qquad \text{(IV.8)}$$

Since $\Sigma < \psi_i | \psi_i >$ is a constant by normalization.

This shows that each ψ_i is an eigenstate of the Hamiltonian, the partial derivative of the Kohn-Sham energy with respect to the position of an ion gives the real physical force on the ion. The result is usually referred to as the Hellmann-Feynman theorem [28,38]. The Hellmann-Feynman theorem holds for any derivative of the total energy. Hence, when each ψ_i is an eigenstate of the Hamiltonian, only the explicit dependence of the energy on the size and the shape of the unit cell has to be calculated to determine the integrated stresses.

Consequences of the Hellmann-Feynman theorem

The Hellmann-Feynman theorem simplifies the calculation of the physical forces on the ions and the integrated stresses on the unit cell. However, the electronic wave functions must be eigenstates of the Kohn-Sham Hamiltonian for the Hellmann-Feynman theorem to be applicable. Therefore the forces on the ions should not be calculated until the electronic configuration is near its ground state. Once the forces and stresses have been calculated, the positions of the ions or the size and shape of the unit cell are changed, the electrons must be brought to the ground state of the new ionic configuration in order to calculate forces and stresses for the new ionic configuration. When the ionic configuration is relaxed to a local energy minimum, the relaxation of the electronic configuration can be partially overlapped with the initial relaxation of the electronic configuration. Provided that the magnitude of the Hellmann-Feynman forces are larger than the errors in the forces, moving each ion the direction of the calculated force will lower the total energy of the system and move the ionic configuration towards the local energy minimum. However if the Hellmann-Feynman forces are smaller than the errors in the forces, displacement of the ions in the directions of the forces may not decrease the total energy and could take the ionic configuration away from the global energy minimum. In this case, overlapping the ionic configuration with the relaxation of the

electronic relaxation will increase the total number of iterations needed to relax the system to the global energy minimum.

However, it might be argued that, as long as the kinetic energy is continuously removed from all degrees of freedom in the system, the total energy in the system must continuously decrease, so that the ionic configuration must relax to a local minimum. This is only true if the time steps are made sufficiently short. Moving the ions a finite distance can add energy to the electronic system. If the energy added to the electronic system in each time step becomes too large, the electronic system will never relax to its ground state, and the ionic system will never reach a local minimum. Therefore some caution has to be exercised when one overlaps ionic relaxation with the electronic relaxation, to ensure that the ionic system reaches the local energy minimum in the shortest possible time.

IV.8 The APW and the LAPW method

There are two things to be taken into consideration when choosing a basis set. First, the basis functions should be as mathematically simple as possible, in order to simplify the setup of matrix elements. The other important feature is to have basis functions that are well suited to describe the system of interest. In 1937 Slater used the muffin-tin approximation as a starting point, he constructed a set of basis functions called augmented planewaves [2,17,18]. In the muffin-tin approximation the crystal is divided into the muffin-tin region consisting of non-overlapping spheres centered around each atomic site, and the surrounding space called the interstitial, the potential is almost spherically symmetric in the muffin-tin region, it will be flat in the interstitial. In the Augmented planewaves method both the simple planewaves and the exact solutions of the Schrödinger equation for a spherical potential are combined to produce very good set of basis functions for describing the electronic structure everywhere in a crystal potential.

The exact APW eigenvalues can be found using information from the eigenvalues of the APW secular matrix which provide a more efficient scheme to solve the APW eigenvalue problem than the traditional evaluation of the secular determinant [2].

One augmented plane wave APW used in the expression of $\psi_{\vec{k}}^{n}$ is defined as:

$$\phi_{\vec{k}}^{\vec{k}}(\vec{r},E)=\begin{cases}\dfrac{1}{\sqrt{V}}e^{i(\vec{k}+\vec{K})\vec{r}} & \vec{r}\in I\\ \sum_{l,m}A_{l,m}^{\alpha,\vec{k}+\vec{K}}u_l^{\alpha}(r',E\ )+Y_m^l(\hat{r}') & \vec{r}\in S_\alpha\end{cases}$$

V is the volume of the unit cell. The APW basis set is $\vec{k}$ -dependent as was the plane wave basis set. The position inside the sphere is given with respect to the center of each sphere by $\vec{r}'=\vec{r}-\vec{r}_\alpha$. The length of $\vec{r}$ is $\vec{r}'$ and the angles θ' is ϕ' specifying the direction of $\vec{r}'$ in spherical coordinates, are indicated as $\hat{r}'$. The Y_m^l are spherical harmonics. The $A_{lm}^{\alpha,\vec{k},\vec{K}}$ and E are yet undetermined parameters, E has the dimension of energy. The u_l^α are solutions to the radial part of the Schrödinger equation for a free atom α, and this at the energy E [11].

IV.8.1 The regular LAPW method

The $u_l^\alpha(r',E)$ have to be constructed at the as yet unknown eigenenergy $E=\varepsilon_{\vec{k}}^n$ of the sought eigenstate and this causes a problem in the APW method. The linearized Augmented Plane Wave method enables us to recover $u_l^\alpha(r',\varepsilon_{\vec{k}}^n)$ on the fly from known quantities. Using Taylor expansion

$$u_l^\alpha(r',\varepsilon_{\vec{k}}^n)=u_l^\alpha(r',E_0)+(E_0-\varepsilon_{\vec{k}}^n)\frac{\partial u_l^\alpha(r',E)}{\partial E}\Big|_{E=E_0}+O(E_0-\varepsilon_{\vec{k}}^n)^2 \qquad \text{(IV.9)}$$

Substituting the first two terms of the expansion in the APW for a fixed E_0 gives the definition of an LAPW. But, the energy difference $(E_0-\varepsilon_{\vec{k}}^n)$ is unknown, leading to an undetermined $B_{lm}^{\alpha,\vec{k}+\vec{K}}$ which has to be introduced.

$$\phi_{\vec{K}}^{\vec{k}}(\vec{r})=\begin{cases}\dfrac{1}{\sqrt{V}}e^{i(\vec{k}+\vec{K})\vec{r}} & \vec{r}\in I\\ \sum_{l,m}[A_{l,m}^{\alpha,\vec{k}+\vec{K}}u_l^{\alpha}(r',E_0)+B_{lm}^{\alpha,\vec{k}+\vec{K}}\dot{u}_l^{\alpha}(r'+E_0)]Y_m^l(\hat{r}') & \vec{r}\in S_\alpha\end{cases}$$

The function in the sphere matches the plane wave in value and slope at the sphere boundary. Then both $A_{lm}^{\alpha,\vec{k},\vec{K}}$ and $B_{lm}^{\alpha,\vec{k}+\vec{K}}$ can be determined. Now, if we want to describe

an eigenstate $\psi_{\vec{k}}^{n}$ that has a p character (l=1), the $A_{(l=1)m}^{\alpha,\vec{k},\vec{K}}$ expansion in LAPW's will be large, to keep the $O(E_0-\varepsilon_{\vec{k}}^{n})^2$ term small, choose E_0 near the center of the p band repeating this argument for every physical l (s, p, d, f states, i.e. up to l=3) and for every atom. The final definition of an LAPW is:

$$\phi_{\vec{K}}^{\vec{k}}(\vec{r})=\begin{cases}\dfrac{1}{\sqrt{V}}e^{i(\vec{k}+\vec{K})\cdot\vec{r}} & \vec{r}\in I\\ \sum_{l,m}[A_{l,m}^{\alpha,\vec{k}+\vec{K}}u_l^{\alpha}(r',E_0)+B_{lm}^{\alpha,\vec{k}+\vec{K}}\dot{u}_l^{\alpha}(r',E_l^{\alpha})]Y_m^l(\hat{r}') & \vec{r}\in S_{\alpha}\end{cases}$$

The basis functions can be calculated once and for all with the E_l^{α} being fixed. Compared to a plane wave basis set, the LAPW basis set can be much smaller. $K_{\max}=\dfrac{7.5\leftrightarrow 9.0}{R_{\alpha}^{\min}}\approx 4au^{-1}$, depending on the desired accuracy. The basis set size $P\approx 195$ compared to $P\approx 270$ for planewaves. The size of the LAPW basis set must be increased as compared to that of APW, due to the less physical shape of the augmenting functions, yielding a larger secular matrix [11].

IV.8.2 The APW+lo method

In the APW method a problem arose concerning the energy dependence of the basis set. This problem can be avoided by removing the energy dependence as the cost of a somewhat larger basis set size. In the APW+lo method the basis set will be energy independent and still have the same size as in the APW method. The APW+lo method combines the good features of APW and LAPW+LO. It is known that the APW+lo basis set contains two kinds of functions. The first kind are APW's with a set of fixed energies E_l^{α}

$$\phi_{\vec{K}}^{\vec{k}}(\vec{r})=\begin{cases}\dfrac{1}{\sqrt{V}}e^{i(\vec{k}+\vec{K})\cdot\vec{r}} & \vec{r}\in I\\ \sum_{l,m}A_{lm}^{\alpha,\vec{k}+\vec{K}}u_l^{\alpha}(r',E_l^{\alpha})Y_m^l(\hat{r}') & \vec{r}\in S_{\alpha}\end{cases}$$

This basis set does not give a good description of the eigenfunctions with fixed energies. Therefore, the basis set is augmented with a second type of functions which are

called the local orbitals. They are another type as the one used in connection with the LAPW method. Their definitions are:

$$\phi_{\alpha',lo}^{lm}(\vec{r}) = \begin{cases} 0 & \vec{r} \in S_{\alpha'} \\ [A_{lm}^{\alpha',lo} u_l^{\alpha}(r', E_l^{\alpha'}) + B_{lm}^{\alpha',lo} \dot{u}_l^{\alpha'}(r', E_l^{\alpha'})] Y_m^l(\hat{r}') & \vec{r} \in S_{\alpha'} \end{cases}$$

The ' indicates that all atoms rather than inequivalent atoms are considered. The same set of energies $E_l^{\alpha'}$ is used as for the corresponding APW's $A_{lm}^{\alpha',lo}$ and $B_{lm}^{\alpha'}$ are determined by normalization and by requiring that the local orbital has zero value at the muffin tin boundary Both the APW and the local orbital are continuous at the sphere boundary but for both their first derivative is discontinuous.

To have accurate results, the APW+lo basis set appears to require a size that is comparable to the APW method ($K_{\max} \approx 3.5 au^{-1}, P \approx 130$) which is less than the LAPW+LO method ($K_{\max} \approx 4 au^{-1}, P \approx 200$) P eigenvalues are obtained by a single diagonalization as in LAPW+LO [11].

CHAPTER V

Results and Discussions

V.1 Electronic Properties

V.1.1 Band Structure

Figures (5.1 a,b,c) show the band structures $E(\vec{k})$ of BeS, BeSe, and BeTe respectively. The most important features of the band structures are: the lowest conduction band is represented by the minima E_c and of the highest valence band is represented by the maxima E_v. The minima and maxima are the places where the free electrons and holes are most likely to be found. The valence band edge in each of these materials is located at the zone center ($k = 0$) and is actually composed of three subbands. When spin is neglected. The spin-orbit effect is assumed to be negligible. Consistent with the effective mass concept, the band with a smaller curvature around $k = 0$ is called the light -hole band and the band with a larger curvature around $k = 0$ is called the heavy-hole band. The conduction bands are also composed of a number of subbands. The calculated lattice constants for the Be-based compounds are given in table (5.1), note that there is a good agreement between our parameters and the ones found experimentally [39].

Table- 5.1 Lattice parameter a(Å) of the BeS, BeSe and BeTe

Compound	Expt	Present	LMTO	Pseudo	Pseudo
BeS	4.865	4.839	4.864	4.745	4.731
BeSe	5.139	5.137	5.137	5.037	
BeTe	5.627	5.638	5.626	5.531	

In Be chalcogenides semiconductors, the conduction band minimum occurs at X-point ($k = \frac{2\pi}{a}$ from the zone center along the ΓX direction). As a result, there are two main valence bands (heavy and light valence bands) with the valence band edge E_v. The forbidden band gap E_g is defined as (E_c-E_v).

The Figures (5.1 a,b,c) show the band structures of BeS, BeSe, and BeTe along the high symmetry points in the B3 phase at equilibrium volume. The overall band profile are similar and are in good agreement with earlier results [39]. The lowest band arises predominantly from the chalcogen valence s state and the upper valence bands arise from the chalcogen valence p states with the top occurring at Γ-point. The conduction band

arises from the Be 2s states with the minimum energy occurring at X-point. The calculated values of direct and indirect band gap (Γ-X) for these compounds are given in table (5.2).

Table -5.2 Calculated values of direct and indirect band gaps (Γ-X) for BeS, BeSe, and BeTe versus pressure.

BeS

Pressure (GPa)	Lattice Parameter a (Å)	Direct Band gap (eV)	Indirect Band gap (eV)
0	4.865	5.510	2.899
10	4.737	5.457	2.717
20	4.640	5.401	2.557
30	4.563	5.350	2.413
40	4.498	5.291	2.282
69	4.353	5.116	1.939

BeSe

Pressure (GPa)	Lattice Parameter a (Å)	Direct Band gap (eV)	Indirect Band gap (eV)
0	5.139	4.173	2.453
10	4.986	4.776	2.247
20	4.875	4.827	2.073
30	4.787	4.797	1.918
40	4.715	4.757	1.776
56	4.619	4.734	1.588

BeTe

Pressure (GPa)	Lattice Parameter a (Å)	Direct Band gap (eV)	Indirect Band gap (eV)
0	5.627	3.606	1.868
10	5.409	3.503	1.573
20	5.263	3.401	1.334
30	5.152	3.305	1.132
35	5.105	3.256	1.035
40	5.063	3.216	0.955

These compounds all have indirect band gaps. The minimum in the conduction band occurs at X or along the Γ-X line. The next lowest conduction band minimum occurs at L_{1c} point in BeSe and BeTe, and at the Γ_{15c} in BeS. The third minimum in the

conduction band occurs at the Γ_{1c} point in BeSe, Γ_{15c} point in BeTe, and at L_{1c} in BeS. The Γ and L point minima are close to each other in energy but much higher than the minimum which occurs along the Γ-X line.

Table- 5.3 Energy band gap E_g (Γ – X) in the B3 phase in (eV).

E_g			
Compound	**Calculated**	**Theoretical**	**Experimental[c]**
BeS	2.81	3.78[a], 2.75[b]	› 4.5
BeSe	2.35	3.12[a], 2.4[b]	3-3.5
BeTe	1.74	2.17[a], 1.18[b]	2.7

[a] Reference [40] TB-LMTO-ASA method

[b] Reference [41] pseudo-potential method

[c] Reference [42]

Effect of pressure on the main band gaps:

The results of our calculation for the direct and indirect gaps for BeS, BeSe, and BeTe versus pressure are presented respectively in figures (5.2 a,b,c). We have used Murnaghan equation of state [43] to express our results in terms of pressure rather than lattice constant:

$$P = \frac{B}{B'}\left[\left(\frac{a_0}{a}\right)^{3B'} - 1\right] \qquad \text{(V.1)}$$

a_0 : Equilibrium lattice parameter.

a : The lattice parameter under pressure p

B : The Bulk modulus.

B' : The pressure derivative of the bulk modulus.

Our results show a linear variation of the gap in all Be compounds. However the results also show that the main energy gaps in BeTe vary linearly quicker than in BeS and BeSe

Figures (5.2 a,b,c) represent band structures of Be compounds at the transition volumes. Notice that the BeS and BeSe compounds are still semiconductors with the values of indirect gaps (Γ-X) decrease at 69 GPa for BeS and 56 GPa for BeSe, but BeTe compound shows a structural phase transition at an energy gap of 35 GPa.

V.1.2 Density of Charge:

The electronic charge density is obtained for each band n by summing over the k-states in the band

$$\rho_n(\vec{r}) = \sum_k |\psi_{nk}(\vec{r})|^2 \qquad \text{(V.2)}$$

and the total charge density is obtained by summing over the occupied band.

$$\rho(\vec{r}) = \sum_n \rho_n(\vec{r}) \qquad \text{(V.3)}$$

The calculated charge densities of BeS, BeSe, and BeTe are displayed in Figures (5.5.a,b,c) respectively. The results show that the distribution of the electronic charge is not symmetric, it decreases from cation to anion, when moving from BeS to BeTe, this is closely linked to the decreasing ionicity of the material. This also shows the clear covalent nature of the bond. In fact Be-based compounds have much higher degree of covalency than the other wide band gap II-VI semiconductors such as CdTe or ZnSe.

Figures (5.3.a,b,c) are contour plots of the charge densities of BeS, BeSe, and BeTe respectively. These charge density plots along the (110) plane indicate that most of the valence charge is concentrated around the anion which decrease from S to Te. This decreasing of symmetry observed in the valence charge distribution for these compounds is often associated with the concept of ionicity. This effect is appropriately described by Phillips scale of electronegativities from atoms where (Be=1.50, S=1.87, Se=1.79, and Te=1.47).

Behavior of the charge density under compression:

The figures (5.5.a,b,c) and figures (5.6.a,b,c) show the valence charge density profiles in the (1,1,1) directions at equilibrium volumes and at compressed volumes in the three Be-based compounds in the zinc-blende structure.

These plots show that as the atoms of column VI are changed from S to Te, the compounds become more ionic, i. e., the charge becomes more accumulated on the cation. The observed trend suggests that the relative electron attraction of anion (S, Se, and Te) with respect to cation (Be) in these compounds increases with increasing hydrostatic pressure. Then the ionicities for these Be compounds decreases with increasing pressure.

One can deduct the mechanism of the compositional transition from the coordination number N_c= 4 (Zinc-blende) to N_c= 6 (NaCl) [44].

V.1.3 Density of States (DOS)

The density of state (DOS) corresponding to the band structures shown in figures (5.1.a,b,c) is presented in figures (5.7.a,b,c). The DOS is calculated using the modified tetrahedron method [45]. This is done by dividing the Brillouin zone into 24 tetrahedral cells. As seen in this figure, the total densities of states are quite similar for all three compounds, with some small differences in the profiles. In this DOS diagram, the minimum of the valence-band density of states occurs is at Γ_1 at -5.81 eV for BeS, at -5.83 eV for BeSe and at -10.56 eV for BeTe . The charge density of the lowest valence band has primary s character for all the three Be compounds. The large peak comes primarily from the onset of the second valence band at point L. The charge density of this band is primarily of cation s character, it changes rapidly to p-like character at the top of the valence band. The conduction bands are well separated from the valence bands by an energy gap of the order of 2.89 eV for BeS, 2.45 eV for BeSe and 1.86 eV for BeTe under normal pressure. The bottom of the conduction band is primarily of cation s character.

V.2 Optical Properties

We now turn to the analysis of the optical spectra. The absorptive part of the dielectric function, ε_2 , is shown in figures (5.8.a,b,c). It is seen that ε_2 is rather similar for all the three beryllium chalcogenides. The main feature is a broad peak with a maximum around 20.81 eV for BeS, 20.78 eV for BeSe, and 24.65 eV for BeTe. The maximum is always greater for BeTe than the two other chalcogenides. Our calculated

spectra are quite similar to the spectra in reference [46] , which were obtained with the empirical pseudopotential method.

The trends in ε_2 as a function of chalcogen may be linked to the trends observed in the DOS and band structures. Compare the highest lying valence bands for the three systems and also the lowest lying conduction bands. Our band-resolved optical calculations show that the transitions between these two bands account for almost all structure in the optical spectra at energies below 6 eV. In BeS, these bands show less dispersion than in BeSe and BeTe. This is the reason why the main peak moves to lower energy and becomes sharper as the chalcogen column is traversed downward.

Next, we consider the dispersive part of the dielectric function, ε_1 , for the three chalcogenides, see figures (5.9.a,b,c). The calculated spectra have been obtained by Kramers-Kronig transformation of the shifted ε_2 spectra. The main features are a shoulder at lower energies, a rather steep decrease between 4 and 5 eV, after which ε_1 becomes negative, a minimum and a slow increase toward zero at higher energies. All these features are very well reproduced in the calculated spectra. The structures are more pronounced in the calculated spectra since these are not broadened.

Finally we shortly discuss the spectra obtainable from the dielectric function. As seen in figure (5.9.a,b,c) , ε_1 is zero at 7.03 eV , 6.3 eV, and 5.184 eV for BeS, BeSe and BeTe respectively. If we look at the curves representing the refractive index, figure (5.11.a,b,c), we find local maxima at these energies. On the contrary, in the absorption coefficient spectra figure (5.10.a,b,c) no maximum is present at these energies, since ε_2 is still large at these energies. Higher up, however, all three beryllium compounds show a large peak in the absorption coefficient spectrum. This peak corresponds to ε_1 going through once again, this time becoming positive. At such energies ε_2 is small, and thus the amplitude of the energy loss may become large.

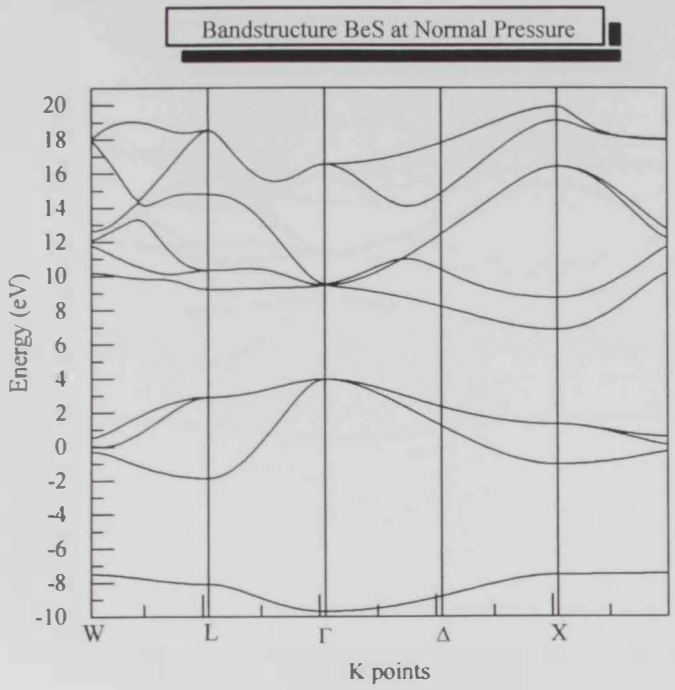

Figure 5.1.a: Bandstructure BeS at Normal Pressure

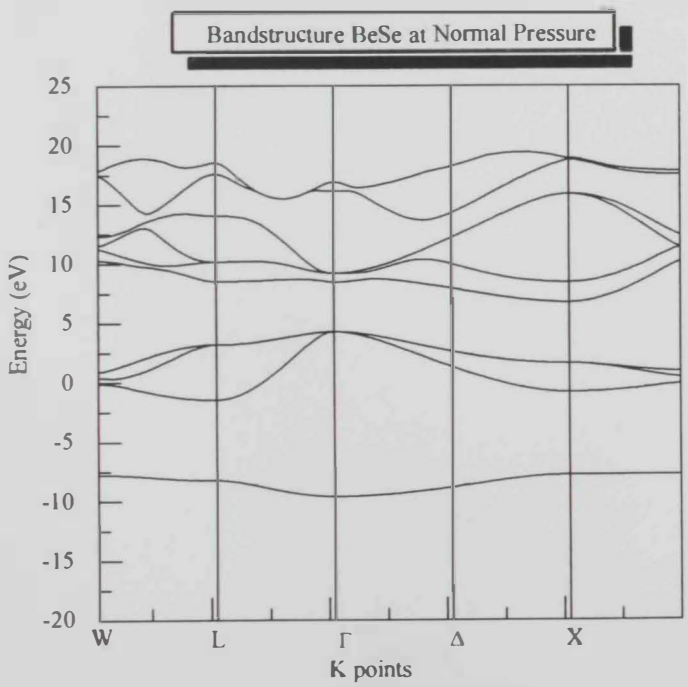

Figure 5.1.b: Bandstructure BeSe at Normal Pressure

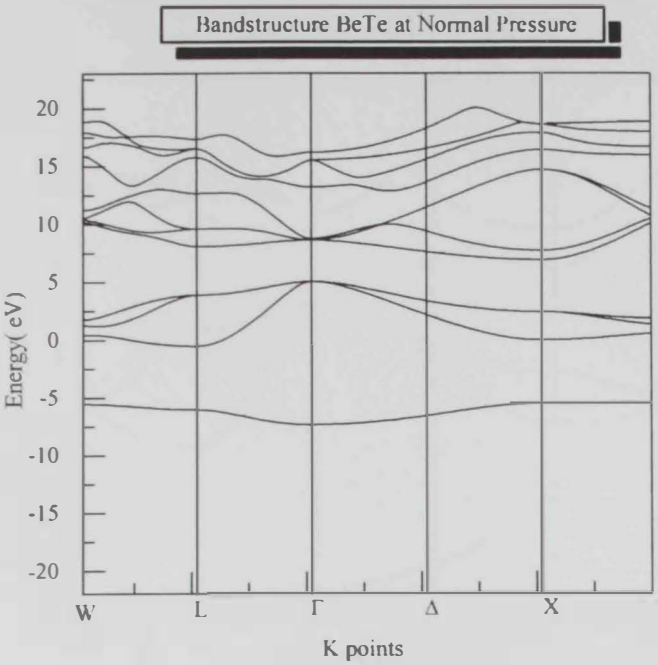

Figure 5.1.c: Bandstructure BeTe at Normal Pressure

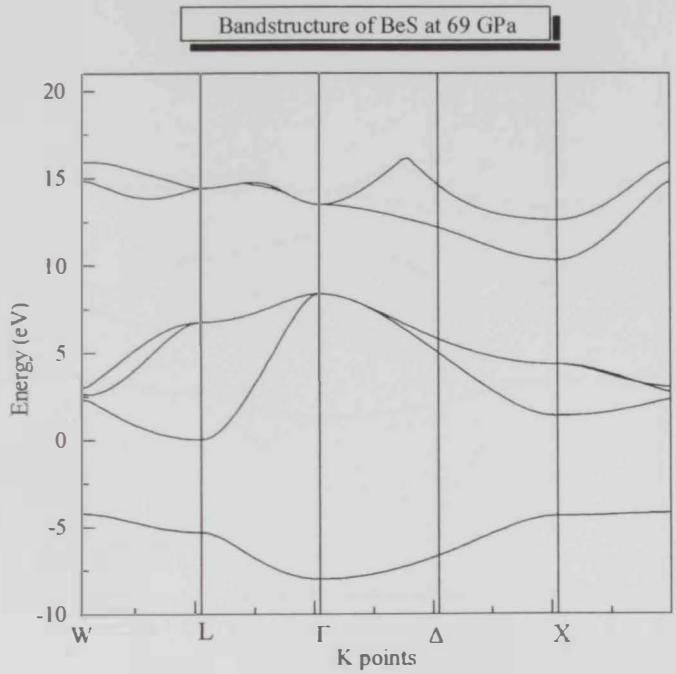

Figure 5.2.a: Bandstructure of BeS at Transient Pressure

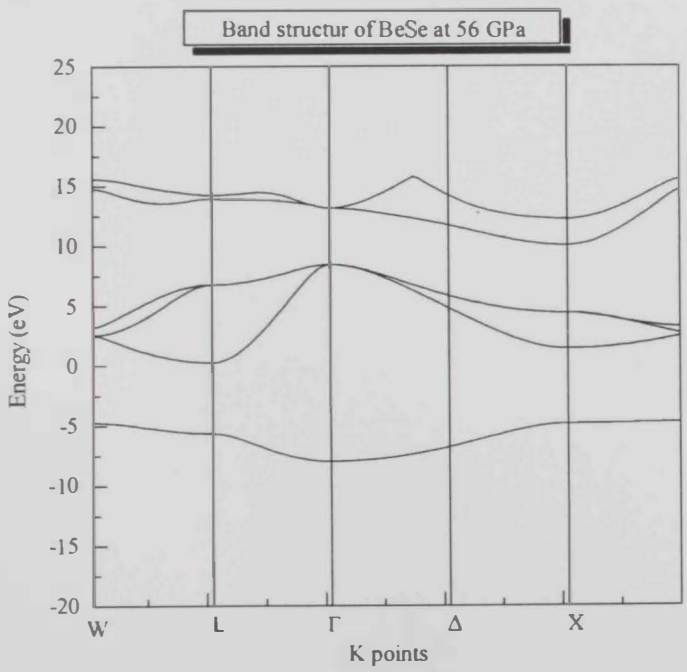

Figure 5.2.b: Bandstructure of BeSe at Transient Pressure

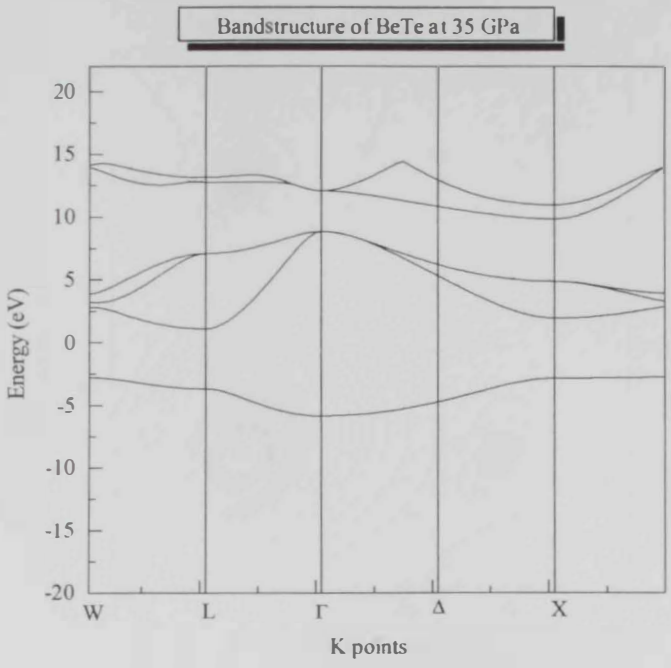

Figure 5.2.c: Bandstructure of BeTe at Transient Pressure

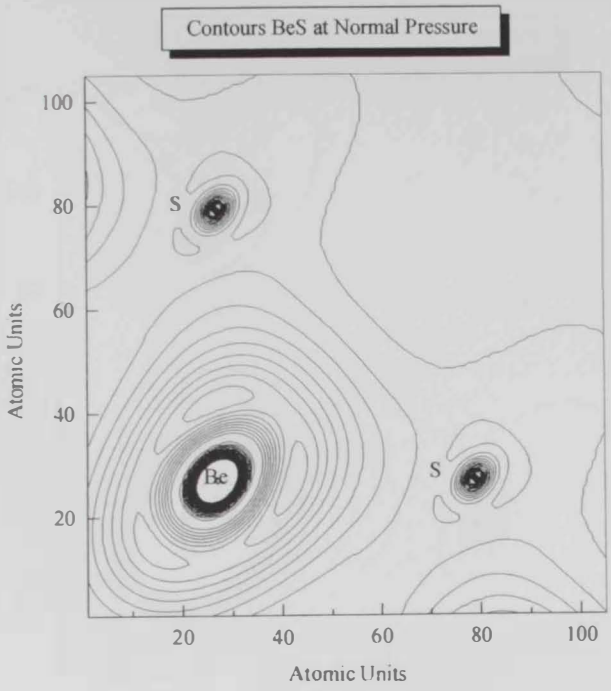

Figure 5.3.a: Contours BeS at Normal Pressure

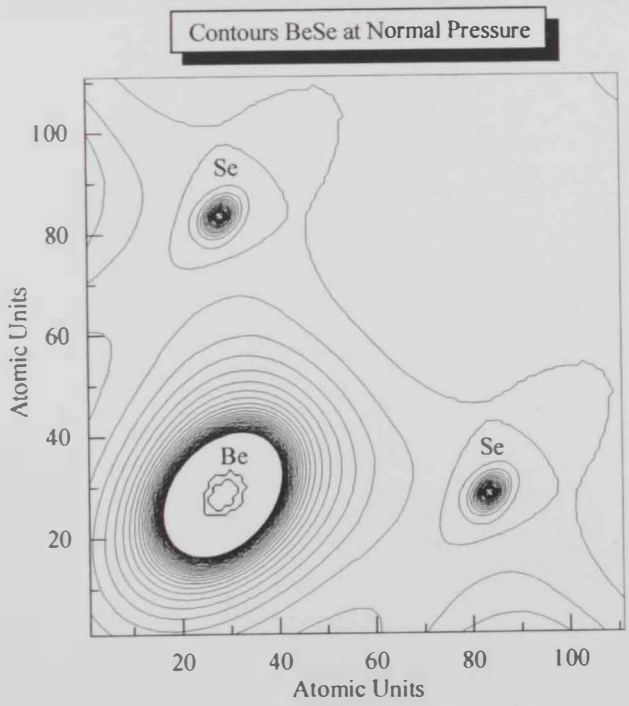

Figure 5.3.b: Contours BeSe at Normal Pressure

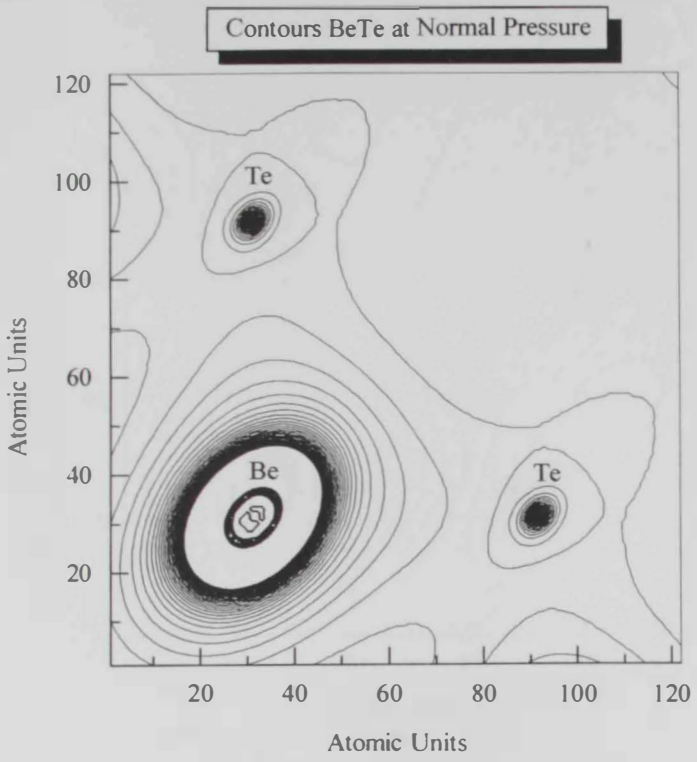

Figure 5.3.c: Contours BeTe at Normal Pressure

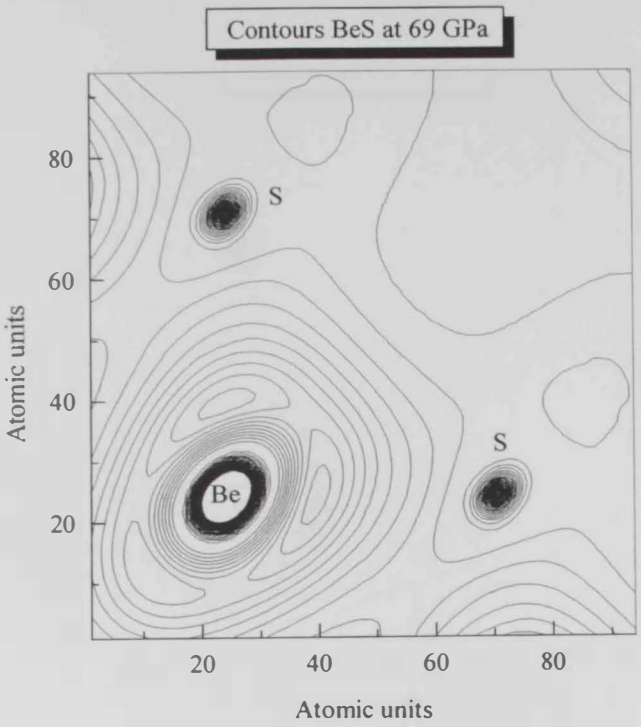

Figure 5.4.a: Contours BeS at Transient Pressure

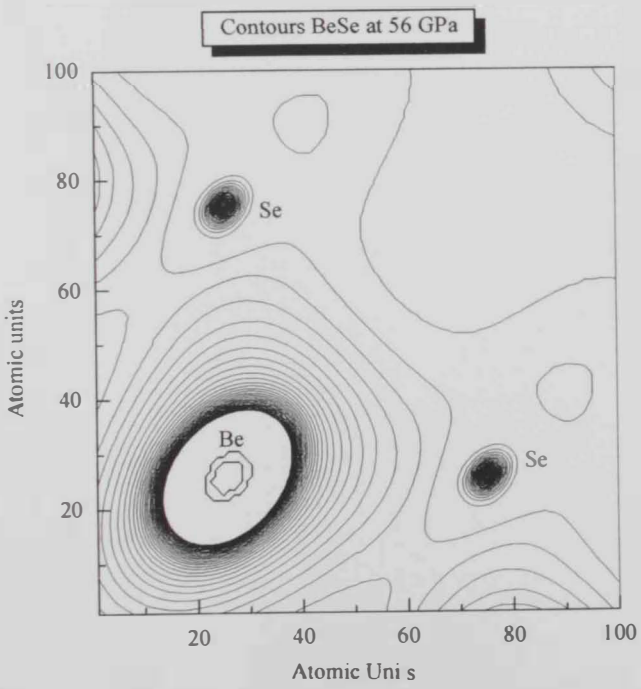

Figure 5.4.b: Contours BeSe at Transient Pressure

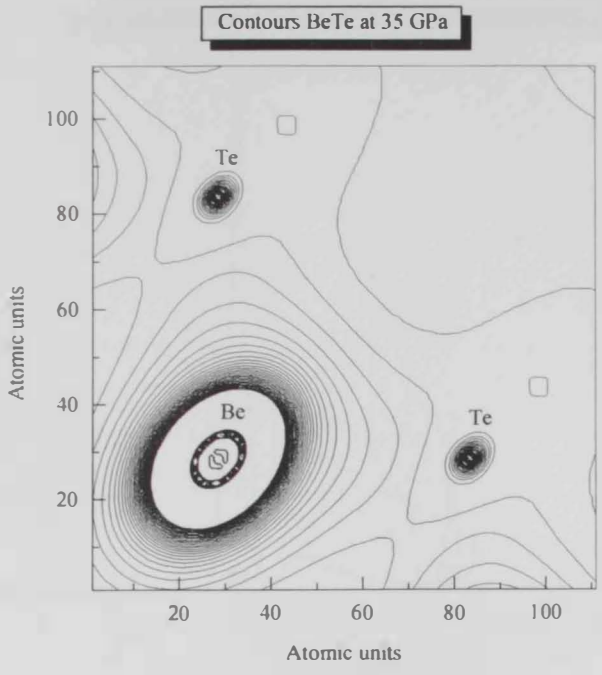

Figure 5.4.c: Contours BeTe at Transient Pressure

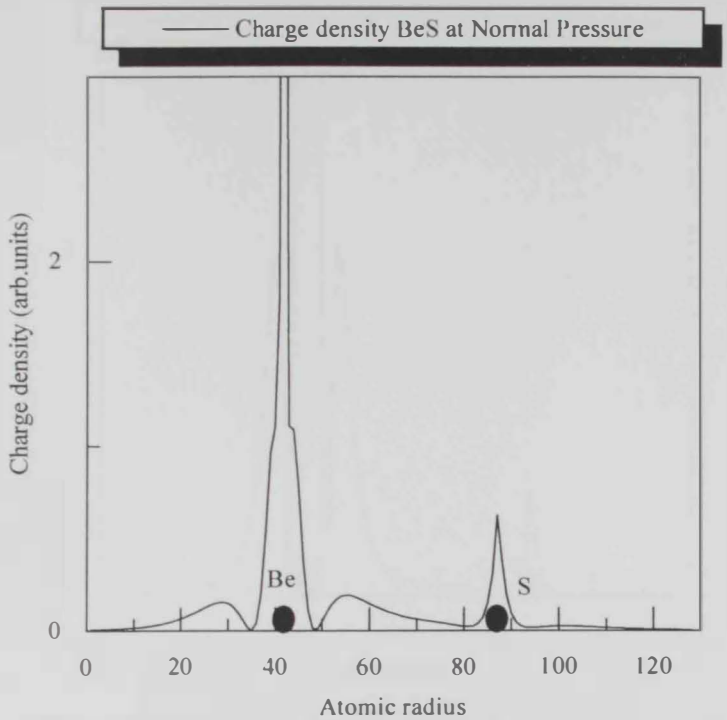

Figure 5.5.a: Charge density BeS at Normal Pressure

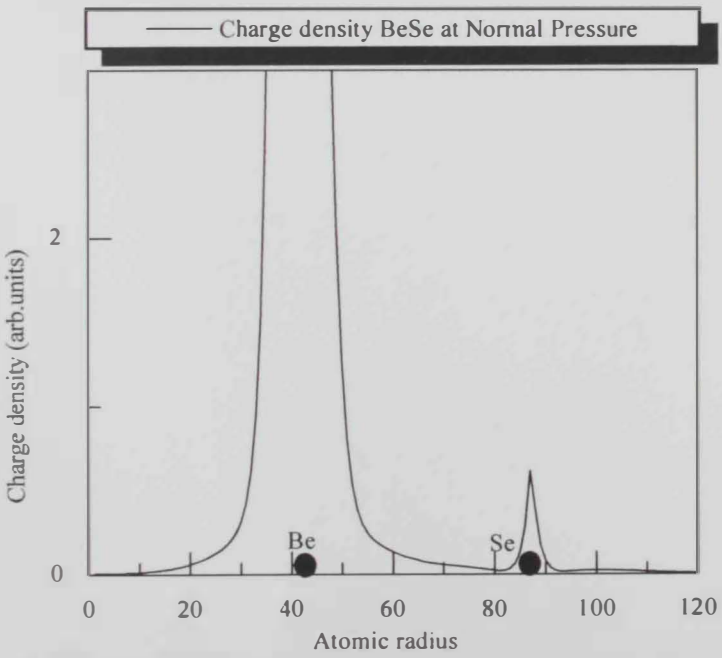

Figure 5.3.b: Charge density BeSe at Normal Pressure

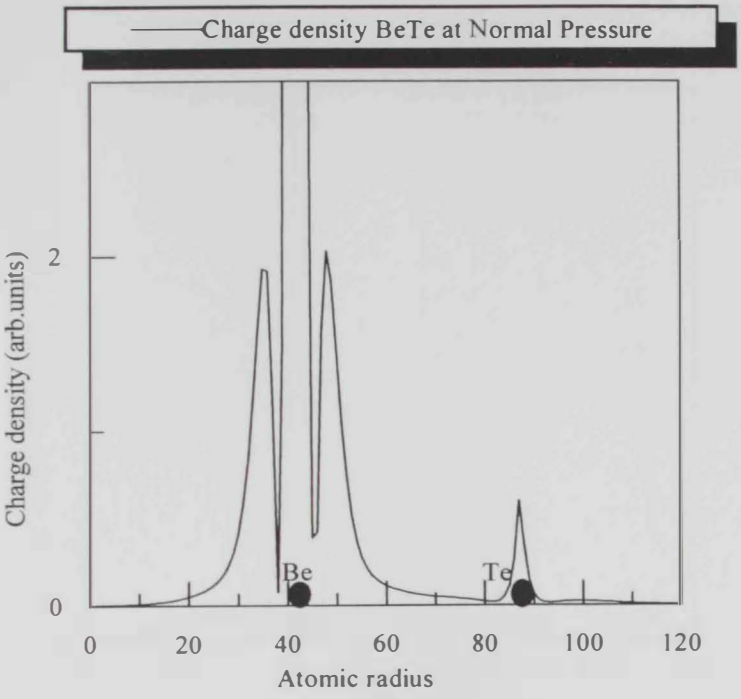

Figure 5.5.c: Charge density BeTe at Normal Pressure

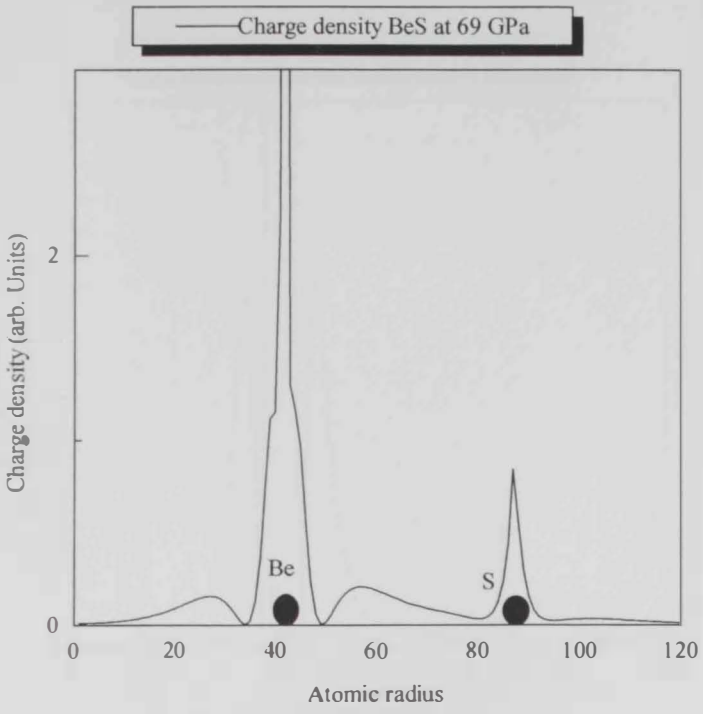

Figure 5.6.a: Charge density BeS at Transient Pressure

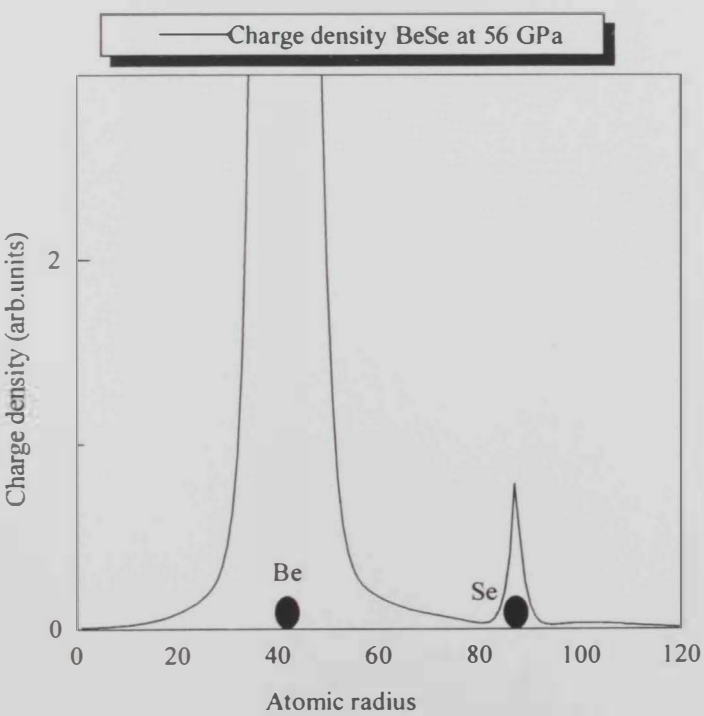

Figure 5.6.b: Charge density BeSe at Transient Pressure

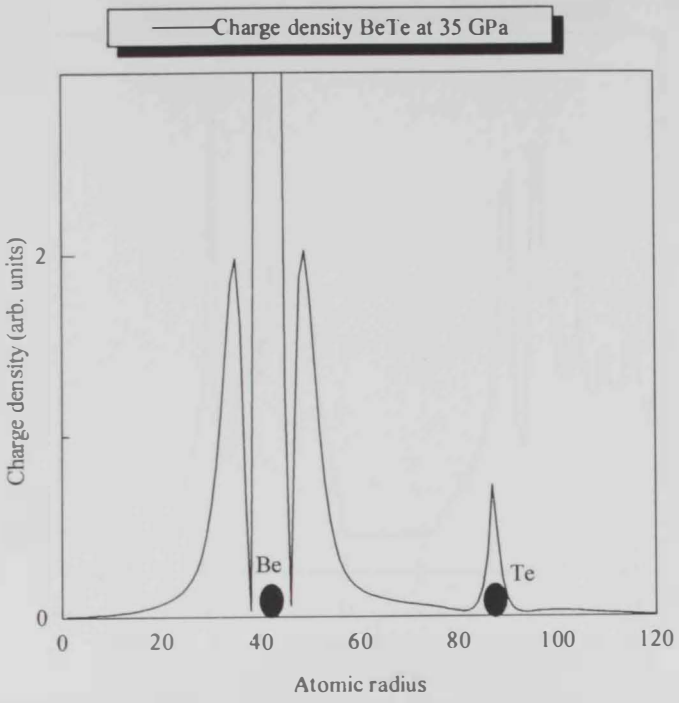

Figure 5.6.c: Charge density BeTe at Transient Pressure

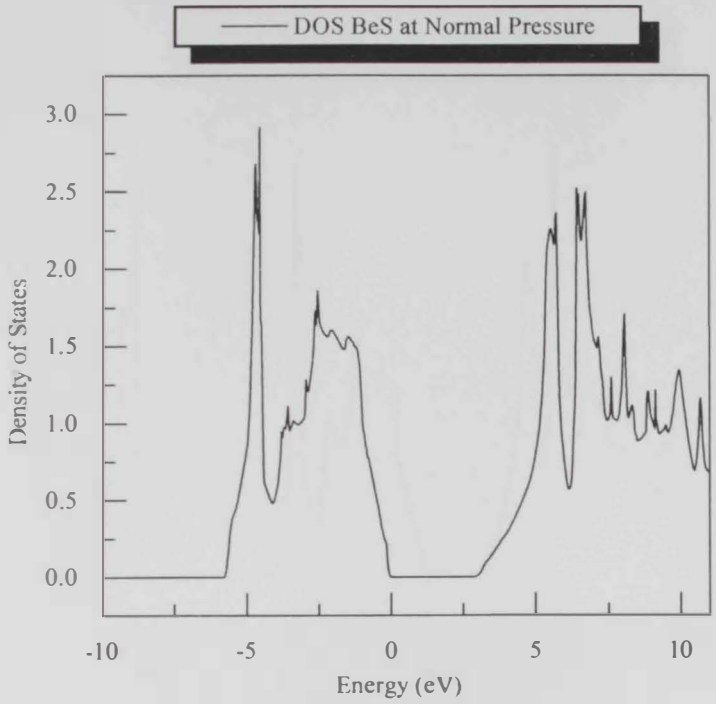

Figure 5.7.a: Density of states of BeS at Normal Pressure

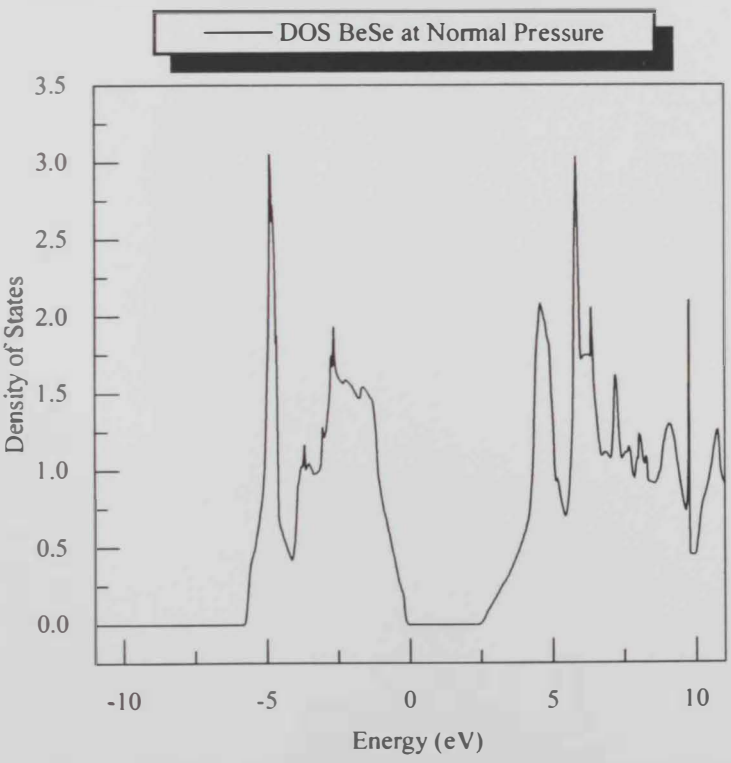

Figure 5.7.b: Density of states of BeSe at Normal Pressure

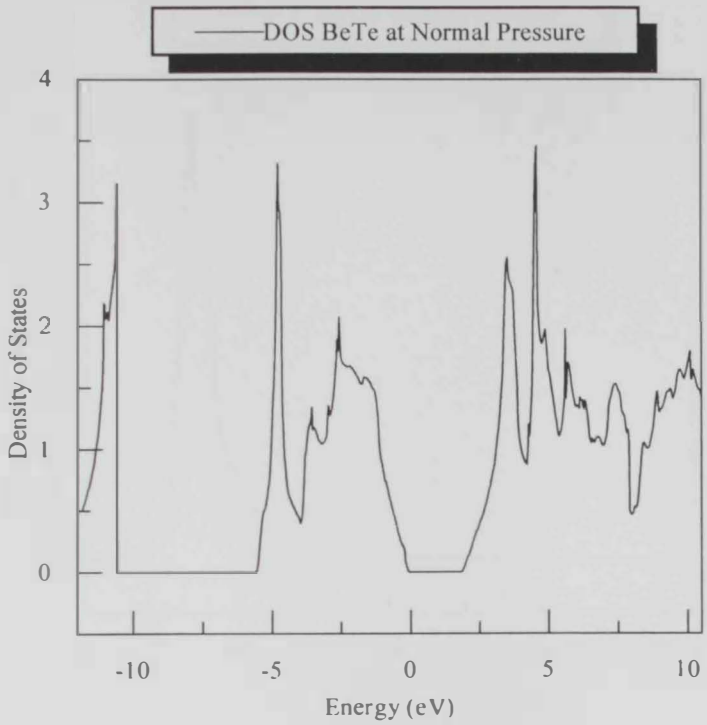

Figure 5.7.c: Density of states of BeTe at Normal Pressure

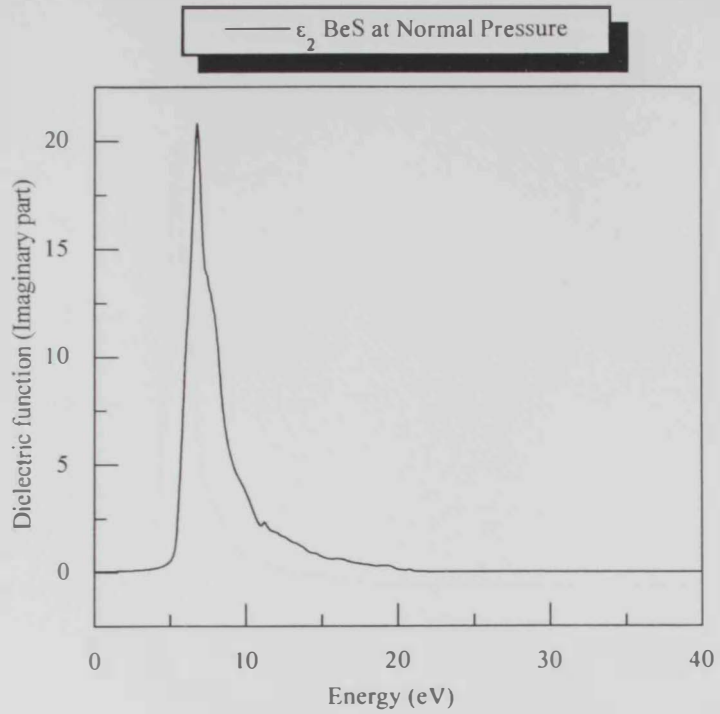

Figure 5.8.a: Imaginary part of Dielectric function of BeS at Normal Pressure

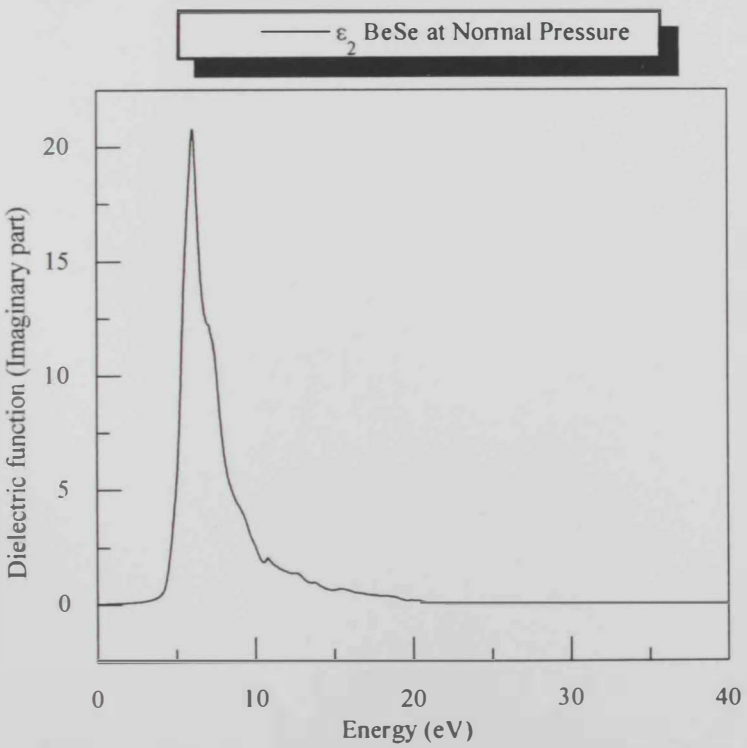

Figure 5.8.b: Imaginary part of Dielectric function of BeSe at Normal Pressure

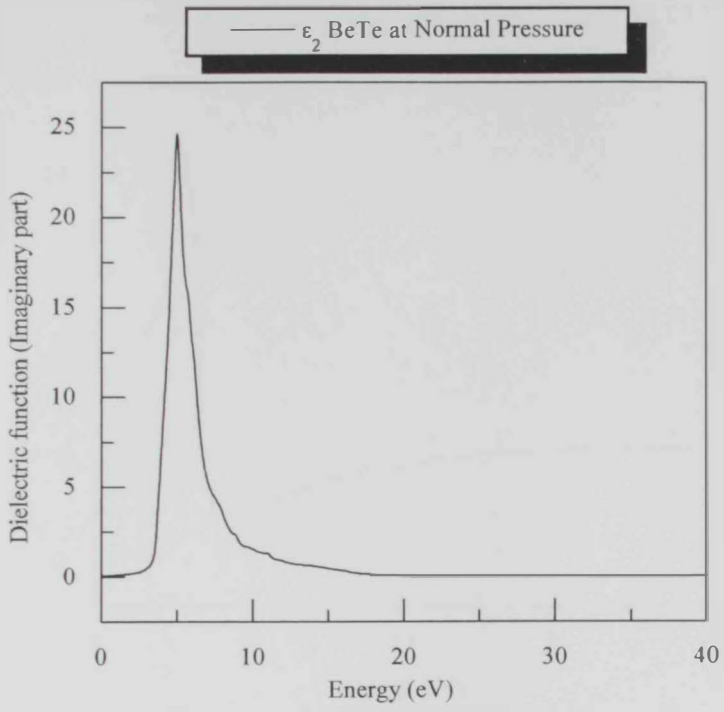

Figure 5.8.c: Imaginary part of Dielectric function of BeTe at Normal Pressure

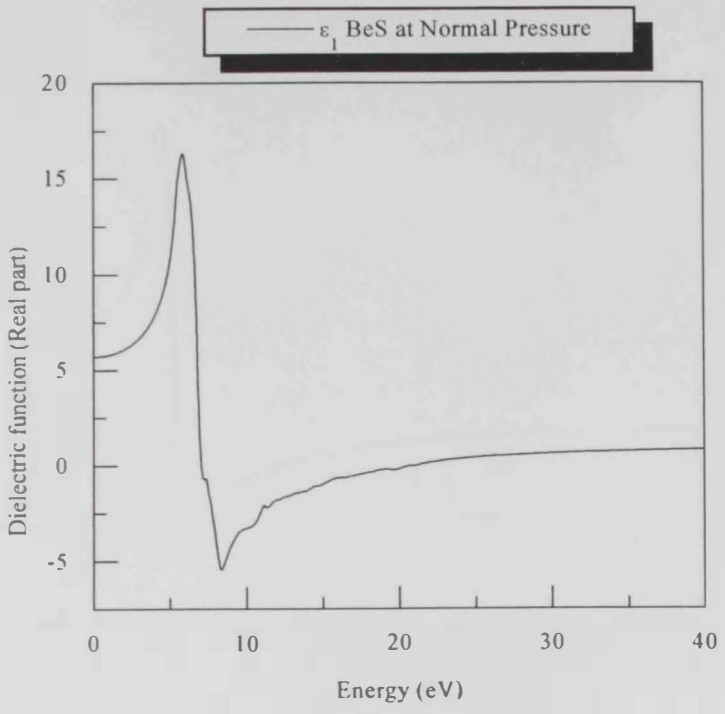

Figure 5.9.a: Real part of Dielectric function of BeS at Normal Pressure

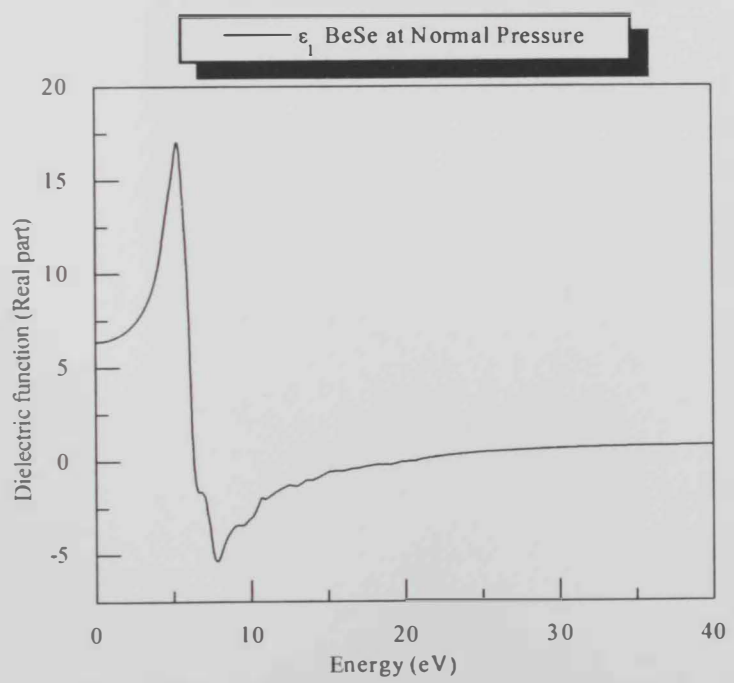

Figure 5.9.b: Real part of Dielectric function of BeSe at Normal Pressure

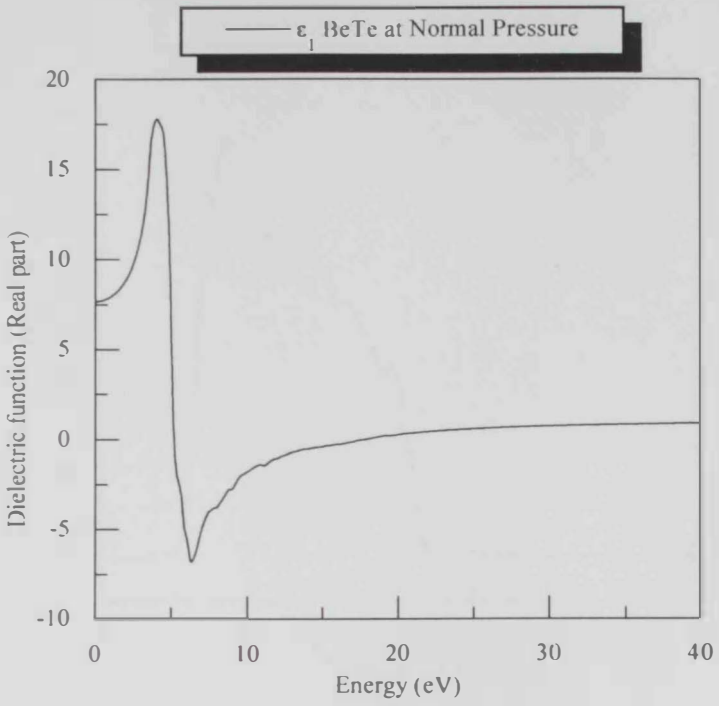

Figure 5.9.c: Real part of Dielectric function of BeTe at Normal Pressure

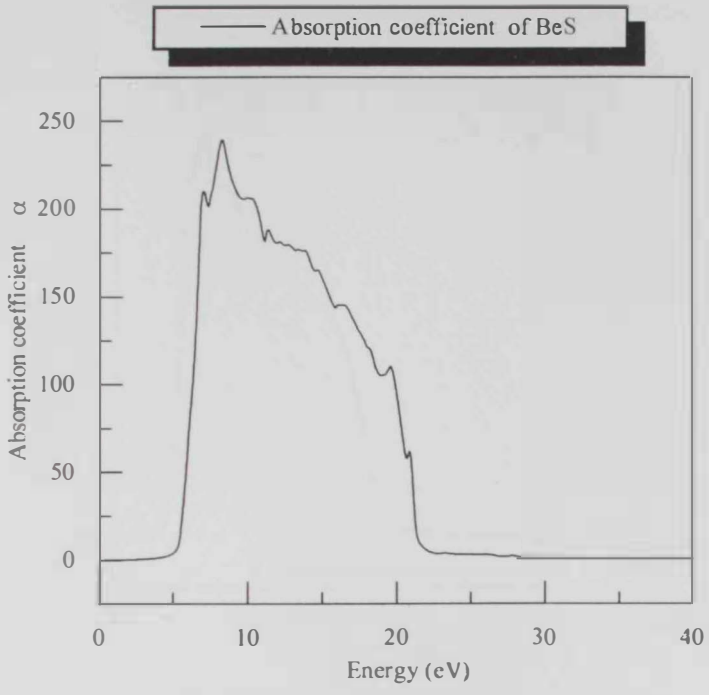

Figure 5.10.a: Absorption coefficient of BeS

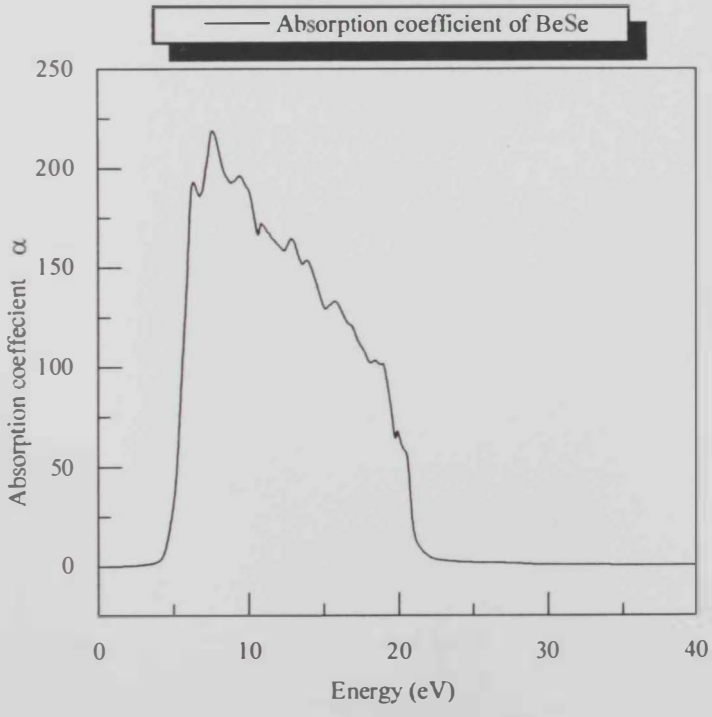

Figure 5.10.b: Absorption coefficient of BeSe

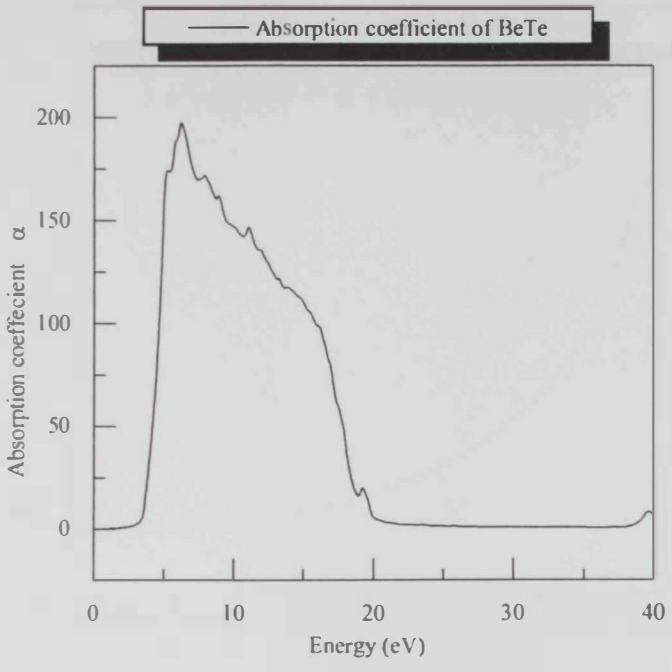

Figure 5.10.c: Absorption coefficient of BeTe

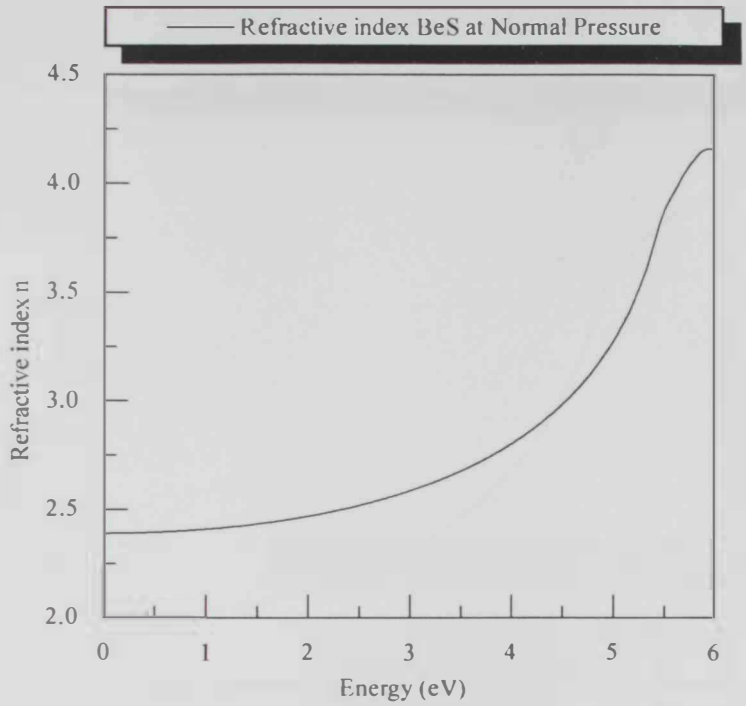

Figure 5.11.a: Refractive index of BeS at Normal Pressure

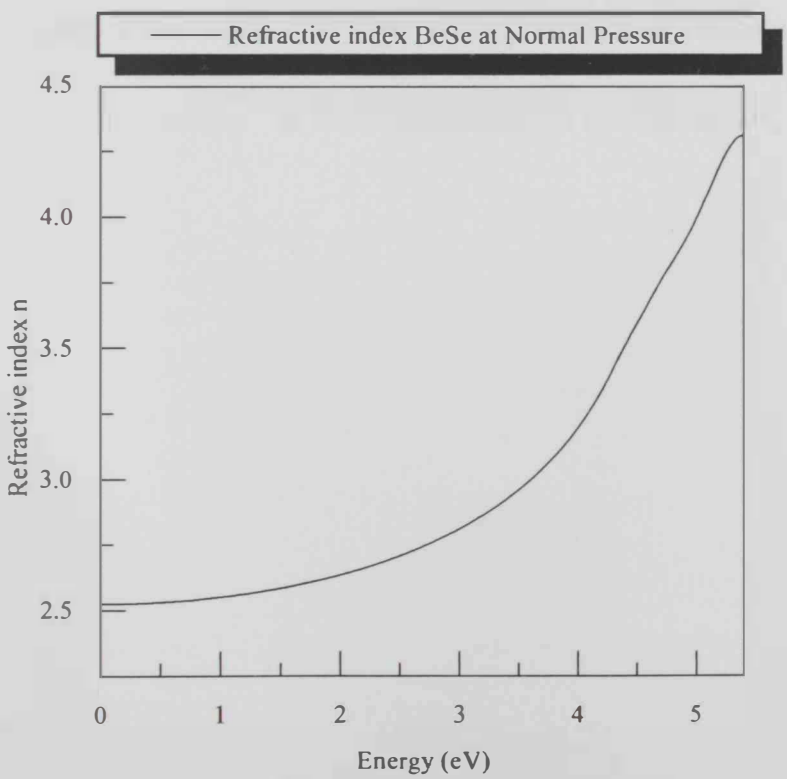

Figure 5.11.b: Refractive index of BeSe at Normal Pressure

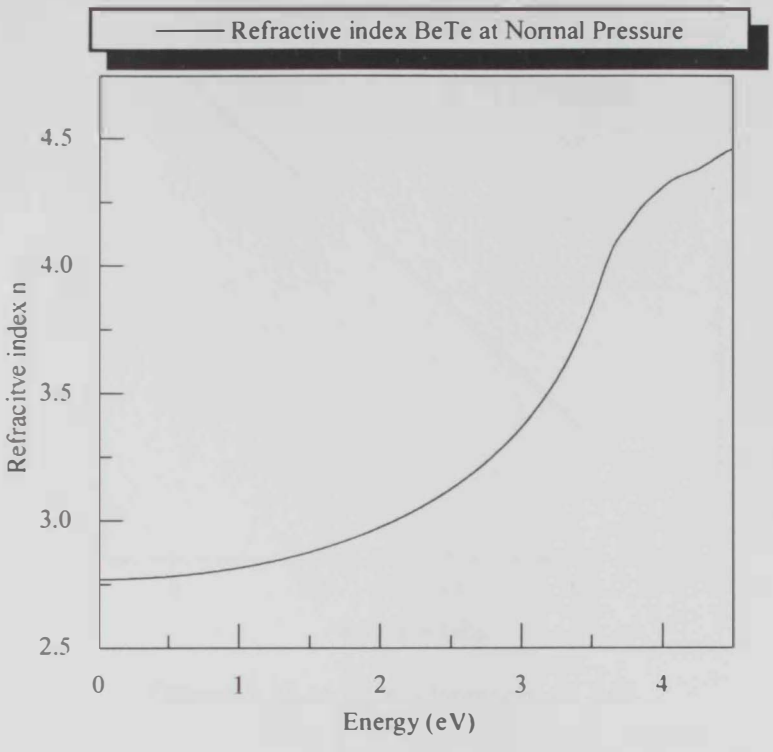

Figure 5.11.c: Refractive index of BeTe at Normal Pressure

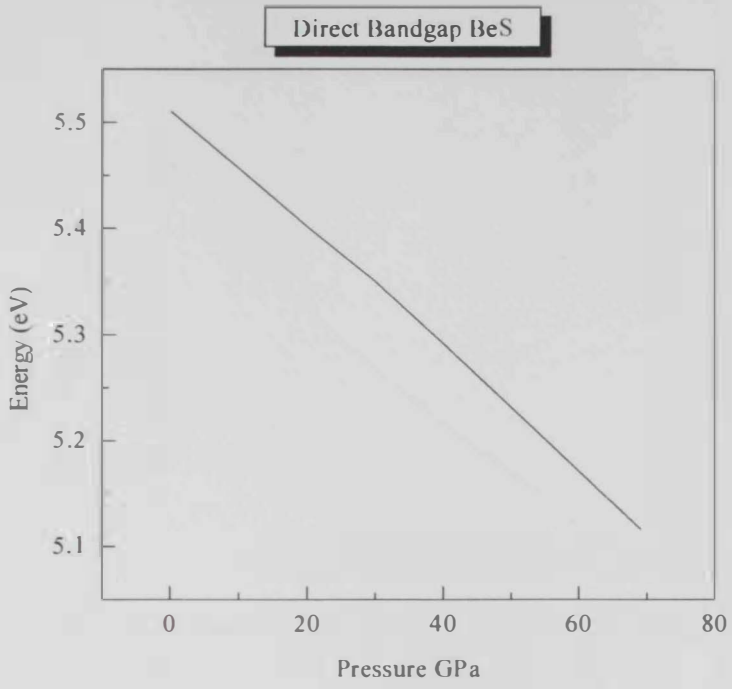

Figure 5.12.a: Direct Bandgap of BeS

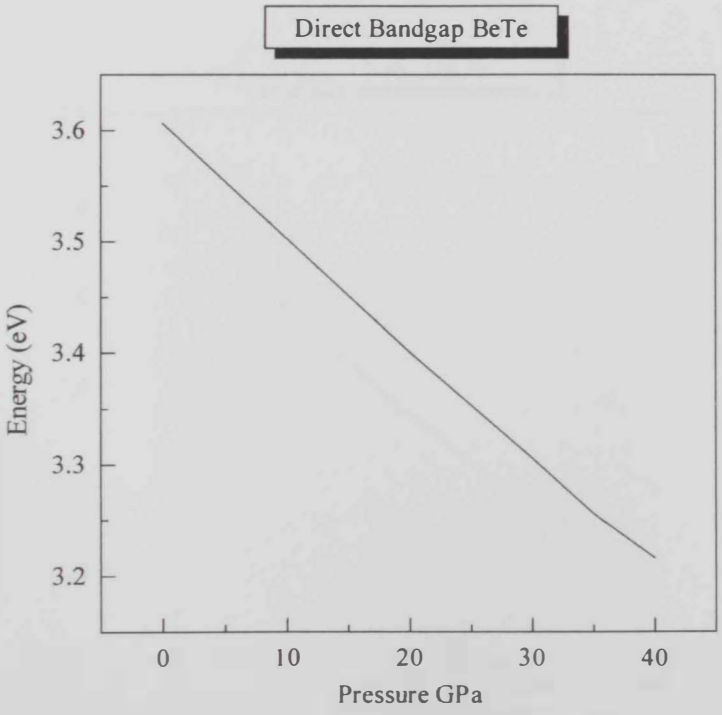

Figure 5.12.b: Direct Bandgap of BeTe

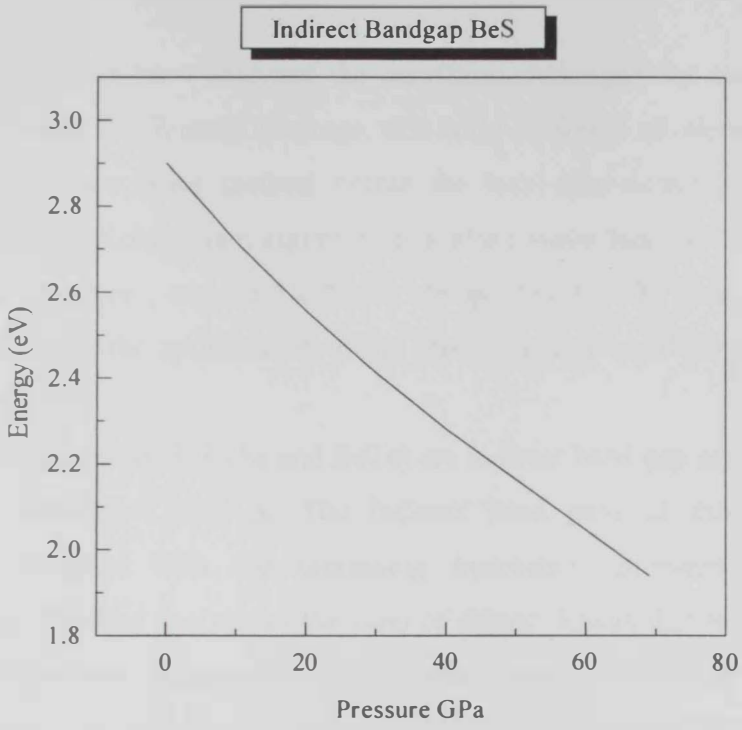

Figure 5.13.a: Indirect Bandgap of BeS

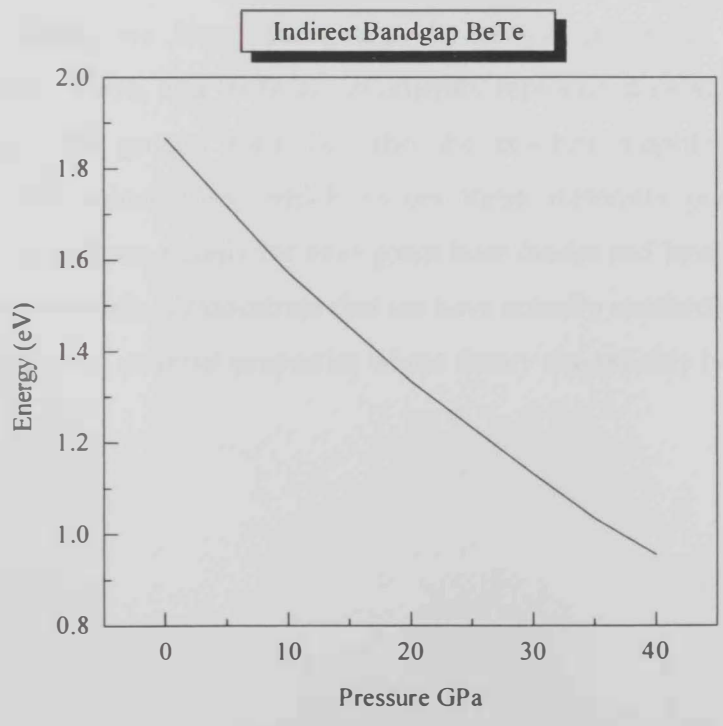

Figure 5.13.b: Indirect Bandgap of BeTe

Conclusion

In this work we have analyzed the beryllium chalcogenides materials in the B3 phase, we have used the Wien2k package, this code performs all-electron full-potential linear-augmented plane wave method within the local-spin density approximation. It solves iteratively the Kohn-Sham equation in a plane wave basis set and computes the electronic band structure , and the electronic charge density. The most time consuming step of the program is the optimization of the wave function coefficients by means of an iterative procedure.

The compounds (BeS, BeSe and BeTe) are indirect band gap semiconductors with gap occurring between Γ and X. The indirect band gaps of the three Beryllium chalcogenides decrease with the increasing hydrostatic pressure as in most of semiconductors. Detailed analysis of the valence charge density distribution confirm that the three chalcogenides compounds are covalent binary compounds. The calculated energy gaps agree well with some other theoretical and experimental techniques. Also the calculated lattice parameters were found to be in good agreement with experimental and theoretical results.

In conclusion, we have shown that the optical properties of the Beryllium chalcogenides BeS, BeSe, and BeTe are excellently reproduced using density functional theory. Not only the general form but also the absolute amplitudes are very well reproduced in our calculations; which makes these materials potentially good for technological applications, mainly for blue-green laser diodes and laser-emitting diodes.

The present results, demonstrate that we have actually reached a level of accuracy for certain fundamental material properties where theory can reliably be trusted.

Appendix A

Basic Concepts of Solid State Physics

A.1 Fourier Transform

Most often, one first encounter with Fourier transform is in the context of time dependent functions. The Fourier Transform (FT) of a function *f(t)* is a function *F(ω)* in frequency domain, defined by:

$$F(\omega) = F\{f\} = \frac{1}{\sqrt{2\pi}} \int_{-\infty}^{\infty} f(t) e^{-i\omega t} dt \qquad \text{(A.1)}$$

$$f(t) = F^{-1}\{F\} = \frac{1}{\sqrt{2\pi}} \int_{-\infty}^{\infty} F(\omega) e^{i\omega t} d\omega \qquad \text{(A.2)}$$

If one would like to construct *f(t)* by adding different functions $e^{i\omega t}$, then *F(ω)* tells what the weight of each function is. For instance, for $f(t) = \cos(\omega_0 t)$ it can be shown that:

$$F(\omega) = \frac{1}{2}\delta(\omega_0 + \omega) + \frac{1}{2}\delta(\omega_0 - \omega) \qquad \text{(A.3)}$$

Therefore, $\cos(\omega_0 t)$ must be equal to a sum of two $e^{i\omega t}$ functions, each with a weight given above:

$$\cos(\omega_0 t) = \frac{1}{2} e^{i(-\omega_0)t} + \frac{1}{2} e^{i\omega_0 t} \qquad \text{(A.4)}$$

which indeed is true, considering the definition:

$$e^{i\omega t} = \cos(\omega t) + i \sin(\omega t) \qquad \text{(A.5)}$$

In this example, there is a discrete set of ω-values where *F(ω)* is non-zero. In general, this is true for any periodic function. Its Fourier transform is nonzero at a discrete set of frequencies (although there might be an infinite number of frequencies in the set). A periodic function can therefore be written as a sum of functions $e^{i\omega t}$. If, *f(t)* is non periodic, *F(ω)* is non-zero over a continuous and often infinite range, and *f(t)* can therefore be written only as an integral over $e^{i\omega t}$ [11].

A.2 The Reciprocal Lattice

The properties of a solid can mainly be investigated the reciprocal lattice vectors. Any property of the solid whether scalar, vector or tensor should have the same periodic translational invariance as the crystalline potential. The primitive vectors of the reciprocal lattice play an important and special role in the Fourier transform of the

physical quantity. The Reciprocal Lattice Vectors have dimensions of inverse distance and are defined in terms of the direct primitive lattice vectors $\underline{a}_1$, $\underline{a}_2$ *and* $\underline{a}_3$. The primitive reciprocal lattice vectors, $\underline{b}^{(i)}$, related to the original lattice vectors via the relations:

$$\underline{a}_i.\underline{b}^{(j)} = 2\pi\delta_i^j \qquad \text{(A.6)}$$

The Kronecker symbol δ_i^j =1 if $i = j$ and zero if $i \neq j$. Thus, the primitive reciprocal lattice vectors are orthogonal to two primitive lattice vectors of the direct lattice. The primitive reciprocal lattice vectors can be constructed via

$$\underline{b}^{(1)} = 2\pi \frac{\underline{a}_2 \wedge \underline{a}_3}{\underline{a}_1.(\underline{a}_2 \wedge \underline{a}_3)} \qquad \text{(A.7)}$$

$$\underline{b}^{(2)} = 2\pi \frac{\underline{a}_3 \wedge \underline{a}_1}{\underline{a}_1.(\underline{a}_2 \wedge \underline{a}_3)} \qquad \text{(A.8)}$$

$$\underline{b}^{(3)} = 2\pi \frac{\underline{a}_1 \wedge \underline{a}_2}{\underline{a}_1.(\underline{a}_2 \wedge \underline{a}_3)} \qquad \text{(A.9)}$$

The denominator is the volume of the primitive unit cell.

The reciprocal lattice consists of the points given by the set of vectors $\underline{Q}$where

$$\underline{Q} = m_1\underline{b}^{(1)} + m_2\underline{b}^{(2)} + m_3\underline{b}^{(3)} \qquad \text{(A.10)}$$

(m_1, m_2, m_3) are integers.

The reciprocal lattice vectors can be considered to be the duals of the direct lattice vectors. This relation can be seen by expressing the primitive lattice vectors $\underline{a}_j$ in terms of the primitive reciprocal lattice vectors $\underline{b}^i$, via

$$\underline{a}_j = \frac{1}{2\pi}\sum_i g_{i,j}\underline{b}^{(i)} \qquad \text{(A.11)}$$

$g_{i,j}$ is given by the metric, since

$$\underline{a}_j, \underline{a}_k = \frac{1}{2\pi} \sum_i g_{i,i} \underline{b}^{(i)} \cdot \underline{a}_k \qquad \text{(A.12)}$$

since

$$\underline{b}^{(i)} \cdot \underline{a}_k = 2\pi \delta_k^i \qquad \text{(A.13)}$$

one has

$$g_{j,k} = \underline{a}_j \cdot \underline{a}_k \qquad \text{(A.14)}$$

The metric tensor expresses the length s of a vector $\underline{r}$ in terms of its component x_i along the basis vectors $\underline{a}_i$. That is, if

$$\underline{r} = \sum_i x_i \underline{a}_i \qquad \text{(A.15)}$$

For a constant metric, the length is given in terms of the components via

$$s^2 = \sum_{i,j} g_{i,j} x_i x_j \qquad \text{(A.16)}$$

The metric tensor, when evaluated in terms of the parameters of the primitive unit cell, is given by the matrix

$$(g_{i,j}) = \begin{pmatrix} a_1^2 & a_1 a_2 \cos\alpha_3 & a_1 a_3 \cos\alpha_2 \\ a_1 a_2 \cos\alpha_3 & a_2^2 & a_2 a_3 \cos\alpha_1 \\ a_1 a_3 \cos\alpha_2 & a_2 a_3 \cos\alpha_1 & a_3^2 \end{pmatrix}$$

The inverse transform is given by

$$\underline{b}^{(i)} = 2\pi \sum_k g^{i,k} \underline{a}_k \qquad \text{(A.17)}$$

$g^{i,k}$ is the metric for the dual vectors.

A.3 Familiar examples

Every physical situation in quantum mechanics is completely defined by its Hamiltonian $\hat{H}$. Every stationary solution of such a problem is described by a state ψ_k

that is an eigenstate of that Hamiltonian. The energy of that solution is the corresponding eigenvalue E_k.

$$\hat{H}\psi_k = E_k\psi_k \qquad \text{(A.18)}$$

The boundary condition in a physical situation limits the possible eigenvalues, and only a discrete set E_k remains. The symbol stands for one or more quantum numbers that are used to label the different eigenfunctions and eigenvlaues that satisfy the boundary conditions [11].

Here, we have an example: The one-dimensional harmonic quantum oscillator

A particle with mass M moves in a one-dimensional harmonic potential $V(x) = \frac{Cx^2}{2}$, the Schrödinger equation for this system is given by:

$$\left(-\frac{\hbar^2}{2M}\frac{d^2}{dx^2} + \frac{Cx^2}{2}\right)\psi_n(x) = E_n\psi_n(x) \qquad \text{(A.19)}$$

The boundary condition is that the particle is bound: its probability to appear at $x \to \infty$ is zero. The discrete set of eigenvalues E_n and eigenfunctions $\psi_n(x)$ can be labeled by a single quantum number $n\,(n = 0,1,2, ...)$ and are

$$En = (n + \frac{1}{2})\,h\nu \qquad \text{(A.20)}$$

$$\psi n(x) = \sqrt{\frac{1}{\sqrt{\pi}\,2^n\,n!}}e^{-\xi^2/2}H_n(\xi) \qquad \text{(A.21)}$$

A.4 Bloch's theorem

Bloch's theorem states that any eigenfunction $\psi(\vec{r})$ can be written as a product of a function $u_{\vec{g}}(\vec{r})$ that has the periodicity of the lattice, and a palne wave $e^{i\vec{g}\cdot\vec{r}}$ with $\vec{g}$ any vector in reciprocal space.

$$\psi(\vec{r}) = u_{\vec{g}}(\vec{r})e^{i\vec{g}\cdot\vec{r}} \qquad \text{(A.22)}$$

As there are an infinite number of vectors in reciprocal space, there are an infinite number of eigenstates of such a Hamiltonian. The wave vectors $\vec{g}$ serve as labels of the eigenstates, and we could therefore rename $\psi(\vec{r})$ into $\psi_{\vec{g}}(\vec{r})$.

Every $\vec{g}$ can be written as the sum of a vector in the first Brilloium zone and a reciprocal lattice vector $\vec{K}$.

$$\vec{g} = \vec{k} + \vec{K} \tag{A.23}$$

Bloch's Theorem can now be rewritten as follows:

$$\psi_{\vec{g}} = \left\{ u_{\vec{g}}(\vec{r}) e^{i\vec{K}.\vec{r}} \right\} e^{i\vec{k}.\vec{r}} \tag{A.24}$$

The function between brackets still has the periodicity of the lattice. We could rename it into $u_{\vec{k}}^{n}(\vec{r})$, where n indicates the number of the Brillouin zone where $\vec{g}$ was in. Indeed n and $\vec{k}$ contain the same information as $\vec{g}$, and can therefore be used as an alternative way of labeling. For n = 1, $\vec{k}$ and $\vec{g}$ are identical. For $\vec{g}$ in the second Brillouin zone, we use the same set of vectors $\vec{k}$, but n is increased to 2, etc. For each $\vec{k}$, an infinite number of n is possible. The parameter n is called the *band index*.

Bloch's theorem can now be restated in its most frequently used form: Any eigenfunction $\psi_{\vec{k}}^{n}(\vec{r})$ can be written as a product of a function $u_{\vec{k}}^{n}(\vec{r})$ that has the periodicity of the lattice, and a plane wave $e^{i\vec{k}.\vec{r}}$ with $\vec{k}$ any vector in the first Brillouin zone:

$$\psi_{\vec{k}}^{n}(\vec{r}) = u_{\vec{k}}^{n}(\vec{r}) e^{i\vec{k}.\vec{r}} \tag{A.25}$$

Actually we have now split off a known part $(e^{i\vec{k}.\vec{r}})$ from the eigenstate, such that only the unknown remainder $u_{\vec{k}}^{n}(\vec{r})$ has to be determined. An important advantage is that this part now known to have the periodicity of the lattice. If a plane wave basis set is used, it can therefore be written as a sum over plane waves that have the same periodicity, and these precisely are the plane waves corresponding to reciprocal lattice vectors

$$u_{\vec{k}}^{n}(\vec{r}) = \sum_{\vec{K}} c_{\vec{K}}^{n,\vec{k}} e^{i\vec{K}.\vec{r}} \tag{A.26}$$

The expansion of $\psi_{\vec{k}}^{n}(\vec{r})$ in the same basis is then

$$\psi_{\vec{k}}^{n}(\vec{r}) = \sum_{\vec{K}} c_{\vec{K}}^{n,\vec{k}} e^{i(\vec{k}+\vec{K})\cdot\vec{r}} \qquad \text{(A.27)}$$

and what have to be searched are the coefficients $c_{\vec{K}}^{n,\vec{k}}$ [11].

A.5 Plane waves

The concept of Fourier transforms can be translated for use with functions $f(\vec{r})$ in real space. In case of spatial function the role of ω will be taken over by so-called reciprocal vectors $\vec{g}$ that have as dimension 1/length. Fourier and inverse Fourier transforms between real and reciprocal spaces are now defined as :

$$F(\vec{g}) = \{f\} = \frac{1}{\sqrt{2}} \int f(\vec{r}) e^{-i\vec{g}\cdot\vec{r}} d^3\vec{r} \qquad \text{(A.28)}$$

$$f(\vec{r}) = F^{-1}\{F\} = \frac{1}{\sqrt{2\pi}} \int F(\vec{g}) e^{i\vec{g}\cdot\vec{r}} d^3\vec{g} \qquad \text{(A.29)}$$

A particular kind of function in real space is a plane wave, defined as:

$$f(\vec{r}) = e^{i\vec{g}_0\cdot\vec{r}} \qquad \text{(A.30)}$$

with $\vec{g}_0$ any vector in reciprocal space. The Fourier transform of a plane wave is non-zero at a single point g in reciprocal space only:

$$F(\vec{g}) = \int e^{i(\vec{g}_0-\vec{g})\cdot\vec{r}} d^3\vec{g} \qquad \text{(A.31)}$$

$$= \delta(\vec{g}_0 - \vec{g})$$

which is very logical, as we need only one function $e^{i\vec{g}\cdot\vec{r}}$ at $\vec{g} = \vec{g}_0$ with weight 1 to build $e^{i\vec{g}_0\cdot\vec{r}}$. The shorter the period of the plane wave in real space is, the further away the point indicated by $\vec{g}_0$ lies from the origin of the reciprocal space.

Functions that are periodic in real space, will have a Fourier transform that is non-zero only at discrete points in reciprocal space (Fourier spectrum). For periodic functions in real space, the Fourier transform will be non-zero over a continuous volume of reciprocal space [11].

A.6 Crystalline solids

In A crystalline solid the potential due to the nuclei is periodic:

$$V(\vec{r}+\vec{R}) = V(\vec{r}) \qquad \text{(A.32)}$$

$\vec{R}$ is any vector of the Bravais lattice. Therefore, if the potential is periodic, the total Hamiltonian is. An infinite solid is built by filling space periodically with copies of the primitive cell. Under these conditions, eigenvalues and eigenfunctions of a periodic Hamiltonian can be labeled with the quantum number n and $\vec{k}$, n = 1, 2, 3, ... and $\vec{k}$ is any vector in the first Brillouin zone that corresponds to a plane wave that is commensurate with the macroscopic crystal. For every valid $\vec{k}$, all values of n occur. The number of valid $\vec{k}$-vectors is equal to the number of unit cells in the macroscopic crystal. For real solids, the $\vec{k}$-vectors are very close to each other, because this number is huge about 10^{23}.

The special $\vec{k}$-vectors that are selected inside the first Brillouin zone are commensurate with the entire macroscopic piece of crystal. Eigenfunctions are written as $\psi_{\vec{k}}^{n}$, eigenvalues as $\varepsilon_{\vec{k}}^{n}$ or $E_{\vec{k}}^{n}$.

The problem here is the eigenvalues are labeled by 4 independent numbers (n, k_x, k_y and k_z), such 4 variables would be needed to make a plot. To solve this problem, an alternative procedure is to select a path through the first Brillouin zone, and plot for every n the energy versus $\vec{k}$. The way the path is selected is usually along the high-symmetry lines in the BZ. Now it is possible to plot the DOS. The DOS is a function of the energy only. Due to the presence of the continuous extra quantum number $\vec{k}$, the definition of the DOS has to be extended:

$$g(E) = \frac{2}{V_{BZ}} \sum_{n} \int \delta(\varepsilon - \varepsilon_{\vec{k}}^{n}) d\vec{k} \qquad \text{(A.33)}$$

Here V_{BZ} is the volume of the first Brillouin zone, and the integral is over the first Brillouin zone. The factor 2 is included to account explicitly for spin [11]. And the $\vec{k}$-vectors are selected from within the bulk of BZ.

Appendix B

Murnaghan Equation of State

B.1 Equations of state:

Formulations

The equation of state (EOS) used in EosFit most commonly used for fitting isothermal (i.e. *P-V* datasets) are listed briefly here. Further details of the derivations and limitations can be found in, for example, Anderson (1995) and Angel (2001)

Murnaghan. This can be derived from the assumption that the bulk modulus varies linearly with pressure, $K = K_0 + K_0' P$; K_0' being independent of pressure. Integration yields the P-V relationship:

$$V = V_0 \left(1 + \frac{K_0' P}{K_0}\right)^{-1/K_0'} \qquad \text{(B.1)}$$

This EOS reproduces P-V data and yields correct values of the room pressure bulk modulus for compressions up to about 10% (i.e. V/V_0>0.9), and has the advantage of algebraic simplicity over other formulations such as the Vinet Birch-Murnaghan EoSs which should be used if the range of compression is greater than 10%. The Murnaghan EoS can also be re-arranged to provide a direct expression for pressure in terms of compression:

$$P = \frac{K_0}{K_0'}\left[\left(\frac{V_0}{V}\right)^{K_0'} - 1\right] \qquad \text{(B.2)}$$

Birch-Murnaghan. This is a "Finite strain EoS", and is based upon the assumption that the strain energy of a solid undergoing compression can be expressed as a Taylor's series in the finite strain, *f*. The Birch-Murnaghan EoS is based upon the Eulerian strain, $f_E = \left[(V_0/V)^{2/3} - 1\right]/2$. Expansion to fourth-order in the strain yields an EoS:

$$P = 3K_0 f_E (1+2f_E)^{5/2}\left(1 + \frac{3}{2}(K'-4) f_E + \frac{3}{2}\left(K_0 K'' + (K'-4)(K'-3) + \frac{35}{9}\right) f_E^2\right) \qquad \text{(B.3)}$$

If this EoS is truncated at second-order in the energy, then the coefficient of f_E must be identical to zero, which requires that K' has the fixed value of 4. The third-order

truncation, in which the coefficient of f_E^2 is set to zero yields a three-parameter EoS (with V_0, K_0 and K') with an implied value of K'' given by:

$$K''=\frac{-1}{K_0}\left((3-K')(4-K')+\frac{35}{9}\right) \qquad \text{(B.4)}$$

Natural strain. Poirier and Trantola developed an EoS based upon the "natural" or "Hencky" measure of linear strain, $f_N = ln(l/l_0)$ which, for hydrostatic compression, may be written as $f_N=1/3ln(V/V_0)$. This yields a pressure-volume relationship expanded to fourth-order in strain of:

$$P=3K_0\left(\frac{V_0}{V}\right)f_N\left[1+\frac{3}{2}(K'-2)f_N+\frac{3}{2}\left(1+K_0K''+(K'-2)+(K'-2)^2\right)f_N^2\right] \qquad \text{(B.5)}$$

Examination of Equation (B.5) shows that truncation of this "Natural strain" EoS at second-order in the strain implies a value of $K' = 2$, different from that of the second-order Birch-Murnaghan EoS. For truncation at third-order in the strain, the implied value of K'' is given by:

$$K''=\frac{-1}{K_0}\left[1+(K'-2)+(K'-2)^2\right] \qquad \text{(B.6)}$$

Vinet. The finite-strain EoS do not accurately represent the volume variation of most solids under very high compression ($\eta<0.6$), so Vinet et al. derived an EoS from a general inter-atomic potential. For simple solids under very high compressions the resulting Vinet EoS provides a more accurate representation of the volume variation with pressure:

$$P=3K_0\frac{(1-f_V)}{f_V^2}\exp\left(\frac{3}{2}(K'-1)(1-f_V)\right) \qquad \text{(B.7)}$$

where $f_V = (V/V_0)^{1/3}$. There is no theoretical basis for truncation of the EoS to lower order, although examination of Equation (B.7) shows that such truncation yields an implied value for K' of 1. The value of K'' implied by equation (B.7) is given by Jeanloz as:

$$K''=\frac{-1}{K_0}\left[\left(\frac{K'}{2}\right)^2+\left(\frac{K'}{2}\right)-\left(\frac{19}{36}\right)\right] \qquad \text{(B.8)}$$

Expansions of the Vinet EoS to include a refineable K' have been proposed but are not required to fit most experimental P-V data simple solids. Despite being often called a "Universal EoS" it should be noted that the Vinet EoS is not intended for materials with significant degrees of internal structural freedom such as bond-bending [40].

B.2 Eigenvalues and eigenvectors

Consider a vector space (IR^n, take n=2 for simplicity) with a basis set $(\vec{e}_1, \vec{e}_2)$ that need not to be orthogonal. With respect to this basis, every vector $\vec{x}$ can be uniquely characterized by two numbers (x_1, x_2). With $\hat{H}$, we denote an operator that can operate on $\vec{x}$, resulting in a new vector $\vec{y} = (y_1, y_2)$:

$$\hat{H}\vec{x} = \vec{y} \tag{B.9}$$

Given $\hat{H}$, we want to find all vectors $\vec{x}$ that under $\hat{H}$ transform into a vector that is parallel with itself:

$$\hat{H}\vec{x} = \lambda\vec{x} \tag{B.10}$$

we rewrite this condition using the basis vectors, and will search for the (x_1, x_2) that satisfy it:

$$\hat{H}(x_1\vec{e}_1 + x_2\vec{e}_2) = \lambda(x_1\vec{e}_1 + x_2\vec{e}_2) \tag{B.11}$$

Left-multiply this equation with $\vec{e}_1$:

$$x_1\vec{e}_1 . (\hat{H}\vec{e}_1) + x_2\vec{e}_1 .(\hat{H}\vec{e}_2) = \lambda(x_1\vec{e}_1.\vec{e}_2 + x_2\vec{e}_1.\vec{e}_2) \tag{B.12}$$

Do the same with $\vec{e}_2$:

$$x_1\vec{e}_2 . (\hat{H}\vec{e}_1) + x_2\vec{e}_2 .(\hat{H}\vec{e}_2) = \lambda(x_1\vec{e}_2.\vec{e}_1 + x_2\vec{e}_2.\vec{e}_2) \tag{B.13}$$

Equations B.12 and B.13 can be summarized in matrix notation as

$$\begin{bmatrix} \vec{e}_1 . (\hat{H}\vec{e}_1) + \vec{e}_1 .(\hat{H}\vec{e}_2) \\ \vec{e}_2 . (\hat{H}\vec{e}_1) + \vec{e}_2 .(\hat{H}\vec{e}_2) \end{bmatrix} \begin{bmatrix} x_1 \\ x_2 \end{bmatrix} - \lambda \begin{bmatrix} \vec{e}_1.\vec{e}_1 & \vec{e}_1.\vec{e}_2 \\ \vec{e}_2.\vec{e}_1 & \vec{e}_2.\vec{e}_2 \end{bmatrix} \begin{bmatrix} x_1 \\ x_2 \end{bmatrix} = \begin{bmatrix} 0 \\ 0 \end{bmatrix} \tag{B.14}$$

The ij^{th} element of the first matrix is a number, as it is the result of a dot product. This matrix is completely determined if the action of $\hat{H}$ on the basis vectors is known. The element of the second matrix are determined by the basis only. This matrix is called the overlap matrix. With this notation, our 2 equations to find suitable (x_1, x_2) become:

$$\begin{bmatrix} H_{11}-\lambda S_{11} & H_{12}-\lambda S_{12} \\ H_{21}-\lambda S_{21} & H_{22}-\lambda S_{22} \end{bmatrix} \begin{bmatrix} x_1 \\ x_2 \end{bmatrix} = \begin{bmatrix} 0 \\ 0 \end{bmatrix} \qquad \text{(B.15)}$$

The left matrix is fully known, apart from λ that is a parameter. For every value of λ, equation (B.15) can be solved for x_1 and x_2. For most values of λ, the determinant of the matrix will be different from zero. Equation (B.15) will have then one unique solution, which is obviously (0, 0). This vector is parallel with the original $\vec{x}$, but in a trivial way. Other, more interesting solutions can occur only for those values of λ that give a vanishing determinant:

$$\begin{bmatrix} H_{11}-\lambda S_{11} & H_{12}-\lambda S_{12} \\ H_{21}-\lambda S_{21} & H_{22}-\lambda S_{22} \end{bmatrix} = 0 \qquad \text{(B.16)}$$

The above equation is called the secular equation of $\hat{H}$. It is a polynomial equation in λ, with as highest power the dimension of the space n. The roots of the secular equation are called the wigenvalues of $\hat{H}$. If $\lambda = \lambda_1$ is an eigenvalue, $[H-\lambda_1 S][x]=[0]$ has an infinite number of solutions: indeed, if (x_1=a, x_2=b) is a solution, ($\beta a, \beta b$) is one too, for β any real number. This conforms with our initial requirement: If $\hat{H}$ transforms $\vec{x}$ into a vector that is parallel with $\vec{x}$, it will do the same with any vector $\beta\vec{x}$. These vectors are called the eigenvectors of $\hat{H}$, belonging to the eigenvalue λ_1. Usually a unit vector among them is chosen to represent this set of vectors. Eigenvectors belonging to different eigenvalues, can be shown to be perpendicular. Therefore, unit vectors belonging to n different eigenvlaues can be taken as an orthonormal basis ($\vec{e}_1^{\lambda_1}, \vec{e}_2^{\lambda_2}$) for the vector space.

What will be the matrix representation of the operator $\hat{H}$, written in this now basis? According to equation (B.14), the matrix elements are:

$$H_{ij} = \vec{e}_i^{\lambda_i}.(\hat{H}\vec{e}_j^{\lambda_j}) \qquad \text{(B.17)}$$

$$= \vec{e}_i^{\lambda_i}.(\lambda_j \vec{e}_j^{\lambda_j}) \qquad \text{(B.18)}$$

$$= \lambda_j \delta_{ij} \qquad \text{(B.19)}$$

This is a diagonal matrix with the former eigenvalues on the diagonal:

$$[H]=\begin{bmatrix}\lambda_1 & 0\\ 0 & \lambda_2\end{bmatrix} \tag{B.20}$$

We could now try to find the eigenvalues and eigenvectors of this operator in the new basis, using the same procedure as described previously. Obviously we will find the same λ_1 and λ_2 as before, with as eigenvectors (1,0) and (0,1). This illustrates that eigenvalues and eigenvectors are intrinsic properties of the operator, and do not depend on the choice of the basis. If the basis we originally started with was already orthonormal, then the overlap matrix will be a unit matrix. This simplifies equation (B.14).

It could happen that 2 of the roots of the secular equation coincide. In that case, that eigenvalue leads to a plane instead of a line of eigenvectors. There is freedom then to choose two mutually perpendicular basis vectors in that plane, but still they are perpendicular to eigenvectors of the other different eigenvalues [11].

B.3 Basis transformation

Consider an operator $\hat{A}$ with matrix representation A, in a vector space IR^n with a normalized but not necessarily orthogonal basis. This operator transforms every vector into a new vector. Also the basis vectors are transformed, and in this way you can understand that the j^{th} column of A contains the coefficients that express the transformed j^{th} basis vector in the original basis:

$$\begin{bmatrix} \dots\ a_{1j}\ \dots \\ \vdots \\ \dots\ a_{jj}\ \dots \\ \dots\ \vdots\ \dots \\ \dots\ a_{nj}\ \dots \end{bmatrix}_{n\times n} \begin{bmatrix} e^{\alpha}_{1j}=0 \\ \vdots \\ e^{\alpha}_{jj}=0 \\ \vdots \\ e^{\alpha}_{nj}=0 \end{bmatrix}_{n\times 1} = \begin{bmatrix} a_{1j} \\ \vdots \\ a_{jj} \\ \vdots \\ a_{nj} \end{bmatrix}_{n\times 1} \tag{B.21}$$

This provides a practical recipe to find the matrix representation of an operator about which we want that it transforms the basis vectors $\vec{e}^{\,\alpha}_j$ in a new set $\vec{e}^{\,\beta}_j$: express each $\vec{e}^{\,\beta}_j$ in the old basis $\vec{e}^{\,\alpha}_j$, and these expansion coefficients form the columns of A. Note that in this way a non-orthogonal basis can be transformed into an orthogonal basis. If both bases are orthonormal, than the matrix A has special properties [11].

Conversely, the j^{th} column of the inverse matrix A^{-1} contains the coefficients that express the vector $\vec{e}_j^{\,\alpha}$ of the old basis in the new basis of the $\vec{e}_j^{\,\beta}$.

$$A = \begin{bmatrix} \frac{\sqrt{2}}{2} & -\frac{\sqrt{2}}{2} \\ \frac{\sqrt{2}}{2} & \frac{\sqrt{2}}{2} \end{bmatrix} \qquad A^{-1} = \begin{bmatrix} \frac{\sqrt{2}}{2} & \frac{\sqrt{2}}{2} \\ -\frac{\sqrt{2}}{2} & \frac{\sqrt{2}}{2} \end{bmatrix}$$

that rotates every vector of IR^2 counterclockwise over 45°. The old basis $(\vec{e}_1^{\,\beta}, \vec{e}_2^{\,\beta})$. The coordinates of these 4 vectors in both bases are:

	Old	New
$\vec{e}_1^{\,\alpha}$	(1, 0)	$(\frac{\sqrt{2}}{2}, -\frac{\sqrt{2}}{2})$
$\vec{e}_2^{\,\alpha}$	(0, 1)	$(\frac{\sqrt{2}}{2}, \frac{\sqrt{2}}{2})$
$\vec{e}_1^{\,\beta}$	$(\frac{\sqrt{2}}{2}, \frac{\sqrt{2}}{2})$	(1, 0)
$\vec{e}_2^{\,\beta}$	$(-\frac{\sqrt{2}}{2}, \frac{\sqrt{2}}{2})$	(0, 1)

References

[1] R. Armiento, Subsystem Functionals in Density Functional Theory Towards a New Class of Exchange-Correlation Functionals, Royal Institute of Technology, Stockholm. (2002)

[2] E. Sjöstedt, Augmented Planewaves, Developments and Applications to Magnetism, ACTA Universitatis Upsaliensis, Uppsala. (2002)

[3] M. Kabir et al, International Journal of Modern Physics B, Vol. 17, No. 10, 2061-2075. (2003)

[4] I. I. Guseinov et al, Pramana Journal of Physics, Vol. 53, No. 4, 727-731. (1999)

[5] J. Kuang, C. D. Lin, J. Phys. B: At. Mol. Opt. Phys. 30, 2529-2548. (1997)

[6] Y. Mori, T. Ikai, K. Takarbe, Photon Factory Cativity Report 2002 #20 Part B. (2003)

[7] C. H. B. Zhang et al, X-ray studies of BeO to 126, Cornell University, Ithaca.(1996)

[8] C. Narayana, V. J. Nesamony, A. L. Ruoff, Phy. Rev. B. Vol. 56. No. 22. (1997)

[9] D. D. Vvedensky, Quantum theory of electrons in solids, The Blackett Laboratory, Imperical College, London. (2000)

[10] R. Van Leeuwen, Kohn Sham potential in density functional theory, Dissertation Vrije Universiteit, Amsterdam. (1994)

[11] S.Cottenier, Density Functional Theory and the Family of (L) APW-methods: a step-by-step introduction, Institute voor kern-en Stralingsfysica, K.U. leuven, Belgium. (2002)

[12] R. Jones, P. R. Briddon, The Ab initio Cluster Method and the Dynamics of Defects in Semiconductors, To appear in identification of Defects in Semiconductors, ed. M. Stavola. (1997)

[13] C. D. Sherrill, The Born-Oppenheimer approximation, School of chemistry and Biochemistry, Georgia Institute of Technology. (1996)

[14] U. Lundin, Physics of Strong Correlations in Electronic Structure and Model Calculations, Department of Physics, Uppsala University, Sweden. (2000)

[15] K. Burke, Modern density functional theory, Rutgers University. (2000)

[16] D. Marx, J. Hutter, Modern Methods and Algorithms of Quantum Chemistry. Edited by John von Neuman Institute for Computing, Vol. 1 . (2000)

[17] P. E. B. Blochl, C. J. Forst, J. Schimpl, Bull. Mater. Sci., Vol. 26. No.1. (2003)

[18] M. Peterson et al, Computer Physics Communication 126, 294-309. (1999)

[19] H. Appel, E. K. U. Gross, Quantum Simulations of Complex Many-Body Systems, John von Neuman Institute for Computing, Vol.10. (2002)

[20] K. Burke, Density Functional Theory and The Meaning of Life, Department of Chemistry, Rutgers University, Piscataway. (2000)

[21] J. Katriel, F. Zahariev, K. Burke, International Journal of Quantum Chemistry, Vol.85, 432-435. (2001)

[22] M. Oppel , DFT- Density functional theory, Austria University. (2002)

[23] C. P. Ewels, Density Functional Modelling of Point Defects in Semiconductors, University of Exeter, Thesis for the degree of Doctor of Philosophy in theoretical Physics. (1997)

[24] A. Lyulin, P. Bobbert, Computational Material Physics (3N290), Amsterdam, Holland. (2004)

[25] M.Grüning, Density Functional theory with improved gradient and orbital dependent functional, VRIJE Univeristeit. (2003)

[26] P. S. Riseborough, Condensed Matter Physics I, University of California at Irvine. (2002)

[27] P. Hessler, J. Park, K. Burke, Phys. Rev. Letters, Vol. 82, No. 2. (1999)

[28] M. Nekovee, W. M. C. Foulkes, R. J. Needs, Phys. Rev. Letters, Vol. 87, No 3. (2001)

[29] A.D. Boese et al, Journal of Chemical Physics, Vol.112, No. 4. (1999)

[30] J. R. Chelikowsky, The Pseudopotential Density Functional Method (PDFM) Applied to Nanostructures, Department of Chemical Engineering and Materials Science, University of Minnesota, (Preprint). (1984)

[31] M. Cote, O. Zakharov, A. Rubio, M. L. Cohen, Phys. Rev. B, Vol. 55, No. 19. (1997)

[32] M. Dur et al, Journal of Applied Physics, Vol. 83, No. 6. (1998)

[33] C. Nayak, Solid State Physics, Physics 140a, University of California, Los Angeles. (2000)

[34] P. R. C. Kent et al, Phys. Rev. B, Vol. 57, No.24. (1997)

[35] C. Makov, R. Shah, M. C. Payne, Phys. Rev. B, Col. 53, No. 23. (1995)

[36] J. Brodholt, American Mineralogist, Vol. 82, 1049-1053. (1997)

[37] A. A. Mostofi et al, Computer Physics Communications 147, 788-802. (2002)

[38] K. Hummer, P. Pusching, C. Ambrosch-Draxl, Excitonic Effects in Anthracene under High Pressure from First Principles, Universitat Graz, Austria. (2003)

[39] G. Kalpana, G. Pari and Abhijit Mookerjee, A. K. Bhattacharyya, Department of Physics, India, Preprint. (2001)

[40] G. Kalphana, G. Prit, A.Mookerjee, and A.K.Bhattacharyya, International Journal of modern physics B, Vol. 12 No 19. (1998)

[41] A. Munoz, P.Rodriguez-Hernandez, and A. Mijica, Phys. Rev B54 11861 (1996).

[42] W.M.Yim, J.P.Dismukes, F.J.Stofko and R.J.Paff, J.Phys. Chem. Solids 33, 501 (1972)

[43] R.J. Angel (EOS-FIT V6.O.), Crystallography Laboratory, Dept. Geological Sciences, Virginia Tech. (2001)

[44] J. S. Dehesa, A. M. Finkelshtein, V. N. Sorokin, Asymptotics of Information Entropies of Some Toda-Like Potentials, Granada University, Spain. (2002)

[45] S. Baroni, Reviews of Modern Physics, Vol.73. (2001)

[46] R. A. Hyman, M.D. Stiles, A. Zangwill, Department of Physics, DePaul University, Chicago, Preprint. (2000)

الملخـــص

هناك عـدّة طرق للعمليات الحسابية التي تجرى على المواد. إحداها Ab initio أو طرق المبـادئ الأولـى التي استخدمت لحل معادلة الكم الميكانيكيّة التي تحكم سلوك النظام، حيث أن حـساب Ab initio للخـواص الإلكترونيّة والضوئية للمواد الصلبة جوهري في فيزياء الحالة الصّلبة. وقد اسـتخدمت طريقـة APW+lo لاختبار الخواص المختلفة لمركبات البريليوم سالفايد، بريليوم سـيلينايد، والبريليـوم تيليرايـد. ومركبـات البريليوم تظهر سمات مختلفـة في بنيتها تحت الضّغوط المختلفة، كما تظهر أيضا مرحلة الانتقال من الشكل المكعب إلى الشكل السّداسي. وحاليّـا هناك اهتمام كبير بدراسة الضّغط المولّد للانتقالات المرحلية لأشـباه الموصّلات المركبة من المجموعتين الثانيـة والسادسة، حيث لا يوجد إلا القليل من المعلومـات عـن هـذه المواد.

الهدف من هذا العمل اختبار الخواص الضوئية والإلكترونيّة لهذه المواد بالتركيز على اعتمادها على الـضغط المتوازن. وقد تم تقسيم العمل إلى جزأين، أوّلا: حسبنا الخواص الإلكترونيّة مثل هيكل الفرقة، كثافة الشّحنة، الشكل الكنتوري لهذه المواد. ثانيا: اختبرنا الخواص الضوئية مثل معامل الانكسار، وظيفة العازل الكهربـائي (بشقيها الحقيقي و الخيالي)، ومعامل الامتصاص تحت الضغط العادي والتحولي. واستخدمنا برنـامجين – Wien97 و Wien2k – لإجراء هذه الاختبارات.

الإشراف على الرسالة

د. نــورالدين عمران

أستاذ مشارك لفيزياء علم المواد
قسم الفيزياء
كلية العلوم - جامعة الإمارات العربية المتحدة

حساب المبدأ الأول Ab initio للخواص الإلكترونية والضوئية لمركبات البريليوم كلكوجينايدز (BeS, BeSe, BeTe) تحت تأثير الضغط

أطروحة مقدمة إلى

عمادة الدراسات العليا

جامعة الإمارات العربية المتحدة

بواسطة

عائشـــة علي سيف بنّان الكعبي

لمتطلبات الحصول على درجة الماجستير في
علوم وهندسة المواد

ديسمبر 2004